

PCCP

Accepted Manuscript



This is an *Accepted Manuscript*, which has been through the Royal Society of Chemistry peer review process and has been accepted for publication.

Accepted Manuscripts are published online shortly after acceptance, before technical editing, formatting and proof reading. Using this free service, authors can make their results available to the community, in citable form, before we publish the edited article. We will replace this *Accepted Manuscript* with the edited and formatted *Advance Article* as soon as it is available.

You can find more information about *Accepted Manuscripts* in the [Information for Authors](#).

Please note that technical editing may introduce minor changes to the text and/or graphics, which may alter content. The journal's standard [Terms & Conditions](#) and the [Ethical guidelines](#) still apply. In no event shall the Royal Society of Chemistry be held responsible for any errors or omissions in this *Accepted Manuscript* or any consequences arising from the use of any information it contains.

Hydrogen bonding and π - π interactions in imidazolium-chloride ionic liquid clusters[†]

Cite this: DOI: 10.1039/x0xx00000x

Richard P. Matthews,^{*a} Tom Welton^a and Patricia A. Hunt^{*a}

Received 00th January 2012,
Accepted 00th January 2012

DOI: 10.1039/x0xx00000x

www.rsc.org/

A systematic electronic structure analysis of hydrogen bonding (H-bonding), anion- π^+ and π^+ - π^+ interactions present in [C₂C₁im]Cl ion-pairs (IP) and selected [C₂C₁im]₂Cl₂ IP-dimers has been carried out. Interactions have been characterised using a combination of QTAIM, NCIPLLOT, NBO and qualitative MO theory. IP-dimers form non-directional charge quadrupolar arrangements due to Coulombic interactions. These are found to associate either as clusters or as loosely associated IP-IP structures. Large conformational changes are found to occur for very little cost in energy, indicating that charge screening is essentially independent of the cation ring orientation. H-bond formation is accompanied by charge transfer and polarisation of the entire [C₂C₁im]⁺ ring. Charge transfer does not follow the same trend for the CHelpG, QTAIM and NBO methods. Weak "stacked" π^+ - π^+ interactions are stabilised in the presence of anions, which locate between and at the periphery of the rings, novel strongly bent H-bonds are also present. Primary (ring; C-H•••Cl⁻) H-bonds and anion- π^+ (C²•••Cl⁻) interactions are found to decay more rapidly with distance than secondary (aliphatic; C^M-H•••Cl⁻) H-bonds. This leads to an increase in the relative importance of secondary H-bond interactions in the IP-dimers. Moreover, rotation of the methyl groups within the "stacked" π^+ - π^+ IP-dimers facilitates the formation of (stronger) linear secondary H-bonds. Thus, compared to isolated IPs, secondary H-bonds may play an increased role within the condensed phase. Overall we find that structural fluidity is facilitated by fluctuating hydrogen bond, π^+ - π^+ and anion- π^+ interactions.

Introduction

π -type interactions including π - π ,¹⁻⁴ CH- π ,⁵⁻⁸ cation- π ⁹⁻¹² and anion- π ¹³⁻¹⁵ have been shown to play important roles in molecular recognition,^{16,17} host-guest chemistry,¹⁸ protein structure,¹⁹⁻²¹ self organised materials²² and nanomaterials.^{23,24} Extensive studies have been carried out to understand the geometric and energetic conditions for stabilising π -type interactions. π - π interactions are dominated by dispersion contributions and are far weaker than both cation- π and anion- π interactions.³ Cation- π and anion- π interactions are comparable in energetic terms; both are dominated by electrostatic and induction contributions.^{3,25} The anion- π interaction includes a small dispersion component which increases with increasing anion size, whereas the cation- π interaction has a minimal dispersion component.³

Only recently have π^+ - π^+ and π^+ - π^+ interactions been recognised as distinctive contributing factors within host-guest chemistry and within the context of fundamental *ab initio* studies of π - π interactions.^{18,25-30} π^+ - π^+ interactions have both the characteristics of conventional π - π and of cation- π systems, but cannot be represented by a simple sum of π - π interactions.²⁵ Moreover, π^+ - π^+ interactions have significant dispersion and electron

correlation components, as found in π - π and π^+ - π^+ interactions. However, a key difference with respect to π - π and π^+ - π^+ interactions is the larger repulsive Coulombic forces exerted by the positively charged π^+ rings on formation of π^+ - π^+ interactions.

ILs are complex fluids composed only of ions that exhibit a favourable combination of physicochemical properties. ILs have been identified as potential replacements for conventional molecular solvents,³¹ leading to an ever-increasing number of IL applications including; in CO₂ capture,³² for the pre-treatment and dissolution of lignocellulose biomass,³³⁻³⁵ as electrolytes for fuel storage and energy devices³⁶⁻³⁸ and as lubricants.³⁹⁻⁴² The optimisation and increased use of ILs for materials applications is dependent on understanding the fundamental interactions present in these liquids.

Coulombic forces dominate in ionic liquids (ILs), wherein charge alternation is a leading characteristic. The isotropic nature of charge-based interactions allows for a considerable assortment of directional secondary intermolecular interactions (i.e. dipole-dipole, dipole-induced dipole, dispersion and H-bonding), which facilitate additional stabilisation and direct the chemistry of an IL.

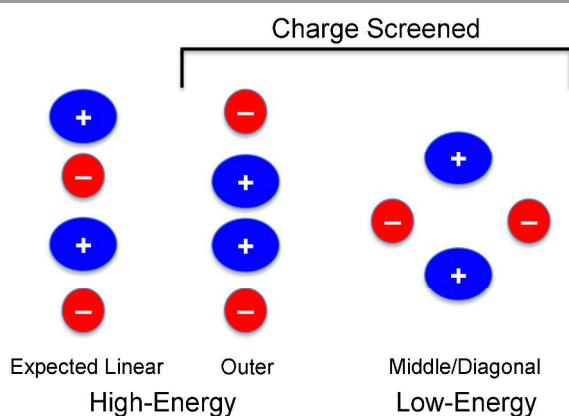


Figure 1: Cartoon representation of charge screening within potential high- and low-energy gas-phase IP-dimer conformers.

π -type interactions have been found to co-exist alongside H-bonding within imidazolium based ILs. π - π stacked motifs have been identified in several IL crystal structures.⁴³⁻⁴⁵ Moreover, the formation of benzene/IL mixtures (liquid clathrates) has been attributed to π - π interactions between the imidazolium cation rings and the benzene molecules.⁴⁶⁻⁴⁸ π - π stacking interactions, with parallel and anti-parallel orientations, have been observed in molecular dynamics (MD) simulations.⁴⁹ Furthermore, a relationship between anion size and π - π stacking has been shown.⁵⁰ *Ab initio* MD simulations have indicated π - π interactions occur in $[C_2C_1im]X$, $X=Cl^-$ and $[SCN]^-$.⁵¹

In π - π systems, charge screening via the inclusion of counterions (**Figure 1**) or a suitable solvent environment (e.g. water) helps to dampen the additional repulsive Coulombic component. Dispersion forces in addition to the Coulombic component play a vital role in determining the favoured low-energy structural arrangements (determined from gas-phase *ab initio* calculations).^{27,52,53} Moreover, highly stabilised π - π structures have been shown to exhibit hydrogen bonding (H-bonding) between the π cations and halides,^{27,52,53} or water molecules in solvated systems.⁵⁴ Thus, indicating that H-bonding is a key component in the stabilisation of low energy π - π structures.

Several π - π stacked motifs have recently been identified for imidazolium based ILs in a computational study of 1,3-dimethylimidazolium chloride ion-pair (IP) dimers, $[C_1C_1im]_2Cl_2$.⁵³ Cation-cation ring stacking structures were described as electron deficient π - π interactions. Moreover, a competitive anion on-top IP motif was also identified as an anion-donor π -acceptor interaction. In a further study, the impact of the anion electronic structure on the disruption of π - π stacked interactions was identified by substitution of the Cl^- anions with a range of larger, charge diffuse anions (i.e. $[NO_3]^-$, $[MeSO_4]^-$, $[OTf]^-$ and $[BF_4]^-$).⁵⁵ These studies highlight the influence of dispersion forces and the importance of H-bonding to the formation of π - π structures in imidazolium based ILs.

The existence and impact of H-bonding on IL structure and properties has been debated.⁵⁶ Extensive theoretical and experimental studies have shown H-bonding to be fundamental to the organisation of ILs.^{53,57-66} Moreover, H-bonding is important in the ability of ILs to dissolve numerous materials,^{67,68} and in molecular solvent/IL^{69,70} and polymer/IL mixtures, e.g. ionogels.^{71,72}

Quantum chemical *ab initio* and density functional theory (DFT) studies of ILs have been generally carried out on cation-anion IPs, as the basic unit of a pure IL. IP structures provide a qualitative understanding of electronic (e.g. charge transfer, dipole moments and electronic polarisability)⁷³ and structural characteristics, including H-bonding and anion- π interactions.^{74,75} However, recent studies have shown that more than one IP is required to expand our understanding of IL systems, in general, and more specifically to study the impact of π - π interactions.^{51,53,76,77}

In this paper we expand the electronic structure analysis of ILs to several IP-dimer structures in order to explore characteristics of the intermolecular interactions; H-bonding, anion- π and π - π interactions. An array of quantum tools is employed, including Quantum Theory of Atoms in Molecules (QTAIM),^{78,79} Natural Bond Orbital (NBO) analysis,⁸⁰ Non-Covalent Interaction (NCI) analysis⁸¹ and qualitative molecular orbital (MO) analysis.

QTAIM examines the topology of the electron density $\rho(r)$ and is considered a robust method for studying H-bonding.^{82,83} QTAIM analysis has also been used to study various π - π type interactions, including cation- π ,^{84,85} anion- π ,^{13,86} π - π ^{87,88} and π - π .⁸⁸ Similarly, NBO analysis has been employed extensively to study the strength and nature of H-bonds,^{80,83} as well as π - π type interactions.^{89,90} Moreover, qualitative molecular orbital (MO) analysis has been employed to understand π - π type interactions.^{55,91}

QTAIM and NBO analysis has been reported for several ILs. These studies have focussed primarily on the H-bonding interactions between the cation-anion IPs and have been restricted to limited conformers with emphasis placed on the lowest energy conformer. For example, QTAIM analysis of one, two and three, Cl^- or Br^- ions in various stable positions around a $[C_2C_1im]^+$ cation,⁹² selected IPs of $[C_4C_1im]Cl^{93}$ and isolated single IPs of $[C_4C_1im]X$ where $X=Cl^-$, $[H_2PO_4]^-$, $[HSO_4]^-$, $[CF_3CO_2]^-$, $[BF_4]^-$ and $[PF_6]^-$ ⁹⁴ have been reported. These studies revealed ρ_b ($\rho(r)$ at a bond critical point) values ranging from 0.016 to 0.050 au for the various anions. Moreover, H-bonds between the methyl substituent (C-H) and the Cl^- anion in $[C_2C_1im]Cl$ IPs revealed appreciable interaction strength, $\rho_b \approx 0.014$ au.⁹² Several IP conformers dominated by anion-donor π -acceptor interactions have also been examined.⁹³ Moreover, a QTAIM study of IP-dimers, featuring $[C_1C_1im]^+$ cations and a range of anions $[X]^-$, $X=Cl^-$, $[NO_3]^-$, $[MeSO_4]^-$, $[CF_3SO_3]^-$ and $[BF_4]^-$, has recently been carried out, with ρ_b values ranging from 0.016 to 0.027 au for the H-bonds.⁵⁵

$E^{(2)}$ values from the NBO analysis are routinely employed to study the strength of $B \cdots H-A$ H-bonds, in particular the $E^{(2)}$

values associated with $n_B \rightarrow \sigma_{AH}^*$ donor-acceptor interactions. Several studies have shown that $E^{(2)}$ values are relatively basis set independent for IL IPs.^{92,95} However, it has been found that $E^{(2)}$ oscillates with increasing cluster size and is dependent on the particular geometric configuration.⁷⁶ Moreover, a decrease in specific $E^{(2)}$ values has been observed on the addition of Cl^- anions for a small number of structures with more than one Cl^- anion around a single $[C_2C_1im]^+$ cation.⁹²

Charge transfer, between the cation-anion IP, and related partial atomic charges is an important descriptor for ILs. Accurate atomic charges are essential for high quality molecular dynamics (MD) simulations.⁹⁶⁻⁹⁸ A simple treatment of charge transfer that has been applied in MD studies is to scale the atomic charges.⁹⁹⁻¹⁰¹ This approach has been shown to improve the dynamic properties of ILs studied, however, the choice of scaling factor is empirical in nature and depends on the IL. Recently, drawbacks inherent in the charge scaling approach have been overcome by the introduction of polarisable force fields, which have shown better agreement with experiment.¹⁰²

Three popular charge partitioning schemes (NBO, CHelpG and QTAIM) have been applied in this work to examine the change in partial atomic charges on moving from $[C_1C_1im]Cl$ IPs to $[C_1C_1im]_2Cl_2$ IP-dimers and to explore the use of charges obtained for IP-dimers, which may better represent the condensed phase.¹⁰³ The partitioning schemes employed, in this work, are fundamentally different. While the results of each method are called "charges" they are different mathematical entities and can be regarded as providing complementary (and sometimes conflicting) information. As with all population methods, mid-range basis sets avoiding the use of diffuse functions should be employed, basis set effects impact on the computation of the electron density or ESP from which the charges are determined. Moreover, trends and not absolute values should be interpreted for similar systems computed using similar methods.¹⁰⁴

In the NBO method natural atomic orbitals (NAOs) are used to form natural bond orbitals that describe a Lewis-like bonding pattern. NAOs are eigenfunctions of the first-order reduced density operator where the eigenvalue represents the occupancy. The eigenfunctions can be expanded using a standard orbital basis set, hence injecting some basis set dependence. The NAOs are local 1e orbitals for an atom given the local molecular environment and effective atomic charge. The NAOs also maintain mutual orthogonality and preserve important nodal features due to Pauli confinement. The NBO method has been recognised as a reliable tool for comparing partial atomic charges and is widely employed.⁸⁰ However, charges tended to be larger than those predicted by other population analysis methods.^{73,104,105} The NBO charges do not present a good ESP, but do represent an isotropic electron density distribution close to the molecule. Higher level partitioning methods can better represent anisotropic distribution of electron density.¹⁰⁶

CHelpG charges are derived from the electrostatic potential (ESP) using a grid-based method. Briefly, a cube of points

(spaced 0.3-0.8 Å apart) that includes a molecule and a 2.8 Å headspace is generated. Points within a predefined van der Waal (VDW) radius of any of the nuclei or outside the 2.8 Å maximum radius are eliminated, the remaining points form a relatively homogeneous layer around the molecule. The ESP at each of the sample points is calculated analytically from the wavefunction and geometry. Then charges on atomic nuclear positions are fit to reproduce these values employing a Lagrange multiplier least-squares routine, which is constrained to fit the overall total molecular charge. A main drawback of the CHelpG scheme is a varying dependence on molecular orientation,¹⁰⁷ a reliance on predefined VDW radii,¹⁰⁸ and poorly fitted interior charges, making this method unreliable for large systems.¹⁰⁵ An advantage is that charges represent the ESP some distance from the molecule and therefore are more suitable to MD force field developments, which depend on a good Coulomb description at long ranges.

QTAIM charges are obtained by analysis of the electron density, which has been calculated from the molecular wavefunction. Topological properties (gradients) are used to divide the electron density into atomic "basins", and integrating over the resultant 3D volume generates an atomic charge. Advantages are that the charge is based on a chemical observable and can be applied to experimentally determined densities.¹⁰⁹ Disadvantages are that the calculations are expensive and charges, as defined for a volume, are not compatible for applications that require nuclei-centred charges.

This work is organised as follows; the naming scheme of $[C_1C_1im]Cl$ IP and $[C_1C_1im]_2Cl_2$ IP-dimers is introduced. The first systematic QTAIM and NBO analysis of $\pi^+-\pi^+$, anion- π^+ and H-bonding interactions in IP-dimer conformers is presented. This is followed by a discussion of charge screening and charge transfer on moving from the IPs to the IP-dimers. A qualitative analysis of the IP-dimer molecular orbitals (MOs) is then carried out, followed by our conclusions.

Computational Details

DFT calculations and population analysis have been carried with the Gaussian 09 (revision D.01) suite of programs.¹¹⁰ All structures have been optimised and confirmed as minima at the B3LYP-D3/aug-cc-pVTZ level. Details of the optimisation procedures are reported elsewhere.⁵³ The importance of including dispersion forces has been recently studied for several IL systems.^{53,111-113} The inclusion of dispersion interactions have been shown to be play a crucial role in correctly describing the $\pi^+-\pi^+$ structures in the systems considered in this work.⁵³ Moreover, dispersion energy corrections have been found to be ≈ 50 kJ/mol for low-energy $\pi^+-\pi^+$ structures.⁵³

Electrostatic potential (ESP) surfaces for selected $[C_1C_1im]Cl$ IPs and $[C_1C_1im]_2Cl_2$ IP-dimers have been generated with the GaussView software.¹¹⁴ Natural atomic orbital (NAO) and natural bond orbital (NBO) analyses have been carried out using the NBO (version 5.9) software.¹¹⁵ All MOs have been generated using the gaussview software at the 0.02 au isosurface. Analysis of the electron density within the

QTAIM framework has been performed on selected $[\text{C}_1\text{C}_1\text{im}]\text{Cl}$ IPs and $[\text{C}_1\text{C}_1\text{im}]_2\text{Cl}_2$ IP-dimers and has been carried out using the AIMALL package.¹¹⁶

QTAIM is based on a topological analysis of the electron density, $\rho(\mathbf{r})$.^{78,79} The topology of $\rho(\mathbf{r})$ is dominated by nuclear maxima, bond critical points (BCPs) which indicate the lowest point of electron density between two nuclei and lines of maximum density (bond paths) linking the nuclear maxima of bonded nuclei. Several properties of the electron density at a BCP have been shown to characterise bonding interactions. These include the electron density (ρ_{\square}), the Laplacian of the electron density ($\nabla^2\rho_{\square}$), and the local electron kinetic (G_{\square}), potential (V_{\square}) and total (H_{\square}) energy densities. The magnitude of both ρ_{\square} and $\nabla^2\rho_{\square}$ at the BCP are linked to the strength of the bond between two nuclei. Moreover, the sign of $\nabla^2\rho_{\square}$ together with the sign of the total energy density (H_{\square}), at the BCP provides further information regarding the nature of the interaction. At the extreme ends of the scale, $\nabla^2\rho_{\square} > 0$ and $H_{\square} > 0$ at the BCP indicate a closed shell interaction, whereas, $\nabla^2\rho_{\square} < 0$ and $H_{\square} < 0$ are indicative of a covalent bond.^{78,79} Two additional critical points; cage critical points (CCP) and ring critical points (RCP), indicate local minima and saddle points of the electron density respectively.

QTAIM topological representations provide a localised atom-atom pair description of chemical interactions and bonding. However, many non-covalent interactions have delocalised character. Thus we have carried out a complementary non-covalent interactions (NCI) analysis, based on the reduced density gradient (RDG, s) and the electron density ρ .¹¹⁷

$$s = \frac{1}{2(3\pi^2)^{1/3}} \frac{|\nabla\rho|}{\rho^{4/3}}$$

This analysis enables identification and characterisation of favourable or unfavourable interactions of various strengths in a semi-quantitative and visual manner. The value of $\text{sign}(\lambda_2)\rho$ is used to colour code RDG isosurfaces. The sign of λ_2 (second contribution to the Laplacian; $\nabla^2\rho = \lambda_1 + \lambda_2 + \lambda_3$) is important, $\lambda_2 < 0$ indicates favourable, $\lambda_2 > 0$ indicates unfavourable and $\lambda_2 \approx 0$ indicates van der Waals interactions. RDG isosurfaces have been generated using the NCIPLOT program⁸¹ and visualised with VMD.¹¹⁸ A density cut-off of 0.1 au was applied and NCI figures have been generated with a isosurface value of 0.35 and coloured in the $[-0.03, 0.03]$ au $\text{sign}(\lambda_2)\rho$ range.

Features of H-bonding can be readily recognised and quantified within the NBO framework via $E^{(2)}$ values which correspond to 2nd order perturbative estimates of donor (filled orbital) to acceptor (empty orbital) interactions,¹¹⁹

$$E^{(2)} = q_i \frac{F_{ij}^2}{\varepsilon_i \varepsilon_j}$$

where q_i is the donor orbital occupancy, ε_i and ε_j are the orbital energies and F_{ij} is the off diagonal NBO Fock matrix element. Distinctive $n_B \rightarrow \sigma_{AH}^*$ donor-acceptor interactions are common to $\text{B}\cdots\text{H-A}$ hydrogen bonding and where electron density is transferred from the H-bond donor, B, into the anti-bonding orbital of the H-bond acceptor, σ_{AH}^* . $E^{(2)}$ values have previously been associated with the degree of covalency, and thus strength, of a H-bond. In this work the sum of the $E^{(2)}$ values are reported. Moreover, H-bonds are classified according to criteria recently outlined for doubly ionic H-bonds within ILs.⁵⁶

Introducing the Ion-Pair Dimers

Structural and electronic characterisation of the IP-dimers ($[\text{C}_1\text{C}_1\text{im}]_2\text{Cl}_2$) can be built up from an understanding of the IPs. The asymmetry of either one or both ions in a cation-anion IP leads to several possible IP conformers.^{57,58,74,120-122} In this work the use of a symmetric $[\text{C}_1\text{C}_1\text{im}]^+$ cation reduces the number of unique anion interaction sites, for the $[\text{C}_1\text{C}_1\text{im}]\text{Cl}$ IPs, to three H-bonding sites (front, side and back) all approximately co-planar with the ring (**Figure 2a**) and one out-of-plane (top) site (**Figure 2b**). The front (0.0 kJ/mol) and top (-1.8 kJ/mol) interaction sites, in $[\text{C}_1\text{C}_1\text{im}]\text{Cl}$ IPs, have been previously shown to be essentially degenerate.^{53,57,74} Moreover, the side (34.3 kJ/mol) and back (61.9 kJ/mol) interaction sites are much higher in energy.

Primary H-bonds have been shown to play an important role in the local ordering and dynamics of ILs.^{58,60,61,64,123,124} However, the role of aliphatic $\text{C-H}\cdots\text{X}$ H-bonds has been less well studied. This type of H-bond has been previously indicated in gas-phase *ab-initio* calculations⁷⁴ and condensed phase MD simulations⁶⁰ and has only recently been confirmed using NMR.¹²⁵ H-bonding interactions with both ring and aliphatic protons have also been indicated in recent studies of IL IP-dimers.^{53,55} Therefore, studies of aliphatic $\text{C-H}\cdots\text{X}$ H-bond interactions are required to determine their distinct role within imidazolium ILs.

In this work primary (1°) H-bonding interactions are defined as those with the ring protons, and secondary (2°) interactions are those with the alkyl chains, **Figure 2**. The anion- π^+ interaction to the C^2 is defined as the T1° (top-primary) interaction.

The front (F) and side (S) IP conformers are each involved in one primary H-bond interaction to the ring protons, e.g. F1° and S1° and one secondary H-bonding interaction to the methyl protons, e.g. F2° and S2°, **Figure 2a**. The top conformer (**Figure 2b**) forms one primary anion- π^+ interaction to the C^2 atom of the $[\text{C}_1\text{C}_1\text{im}]^+$ cation, i.e. T1°, and two equivalent secondary H-bonding interactions to the two methyl protons, both labelled T2°. Moreover, the back (B) conformer (**Figure 2a**) forms two equivalent primary interactions, B1°.

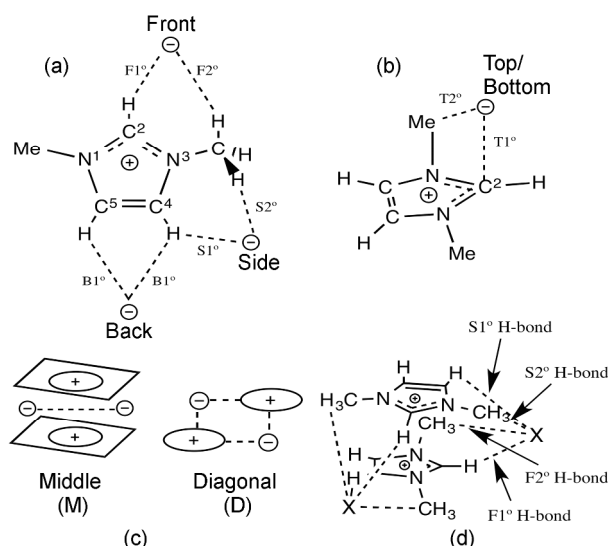


Figure 2. (a) Co-planar (front, side and back) and (b) out-of-plane (top) anion interaction sites around a [C₁C₁im]⁺ cation. (c) General middle and diagonal structural motifs for the [C₁C₁im]₂Cl₂ IP-dimers and (d) illustration of the naming convention applied to the M_{FS}SF_R [C₁C₁im]₂Cl₂ IP-dimer.

Structural and energy data for [C₁C₁im]₂Cl₂ IP-dimers computed with a range of DFT methods has been reported.⁵³ Two low-energy motifs labelled middle and diagonal (**Figure 2c**) were identified and found to exhibit a range of structural conformers with relative conformer energies <10 kJ/mol, at the B3LYP-D3/aug-cc-pVTZ level.

The middle (M) motif is identified by parallel-stacked cations, with the two anions lying in a middle plane, between the [C₁C₁im]⁺ cation rings. Each anion is able to interact with both cations within this arrangement. Moreover a potentially repulsive π⁺-π⁺ stacking interaction, stabilised by the presence of the anions, is achieved.

The diagonal (D) motif is categorised based on the positioning of both anions at opposite diagonals of a rectangle with the [C₁C₁im]⁺ cations occupying the remaining corners. This arrangement maximises the number of in-plane front and out-of-plane top cation-anion interactions, with little possibility of π⁺-π⁺ stacking.

The [C₁C₁im]₂Cl₂ IP-dimer names have been apportioned into four sections. The principal part of the name is taken from the general motif, i.e. middle (M) or diagonal (D). The second and third parts are based on the relative positions of the anions in relation to cation 1 and cation 2 respectively, i.e. front (F), side (S), back (B), top (T) or bottom (Bt). The final element details the relative [C₁C₁im]⁺ cation ring orientations, i.e. parallel (P), rotated (R), antiparallel (A) or T-shape (T).

For example, the M_{FS}SF_R [C₁C₁im]₂Cl₂ IP-dimer is depicted (**Figure 2d**). This structure has a middle (M) arrangement of anions, exhibits alternate front and side (FS and SF) H-bonding interactions between each anion and both cations and the [C₁C₁im]⁺ rings are stacked in a rotated orientation (R).

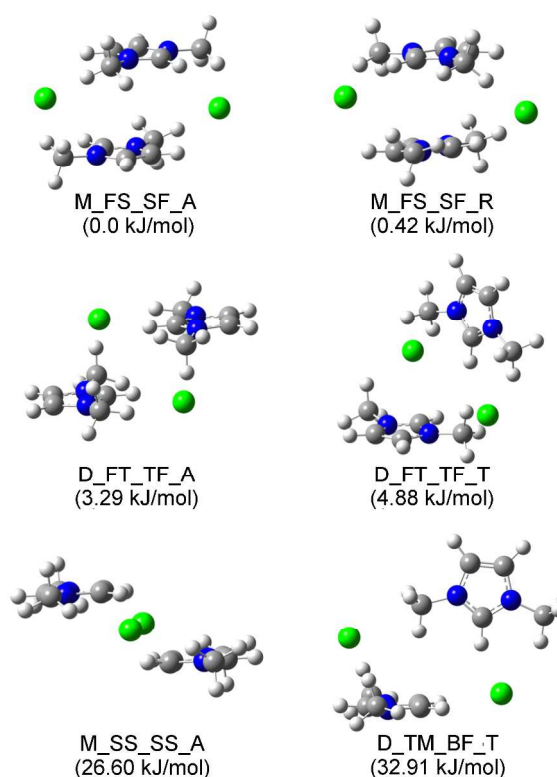


Figure 3: Selected [C₁C₁im]₂Cl₂ IP-dimer conformers. Conformer energies are set relative to the lowest energy structure, M_{FS}SF_A (Binding energy = -909.89 kJ/mol).⁵³

13 structures were identified with relative conformer energies below 50 kJ/mol. Six structurally distinct [C₁C₁im]₂Cl₂ conformers (**Figure 3**) have been selected for electronic structure analysis in order to elucidate understanding of the interplay of fundamental interactions (H-bonding, π⁺-π⁺ and π⁺-Cl⁻) present in these structures. These include the lowest energy M_{FS}SF_A structure and three low-energy (<10 kJ/mol) conformers (M_{FS}SF_R, D_{FT}TF_A and D_{FT}TF_T), which maximise front, top and side IP interactions. Moreover, two medium-energy, D_{TM}BF_T (32.9 kJ/mol) and M_{SS}SS_A (26.6 kJ/mol), conformers that present unique structures exhibiting back and meth⁶⁰ IP interactions, which are stabilised in the [C₁C₁im]₂Cl₂ IP-dimers compared to the isolated IPs, have also been selected. Variations on each of these conformers by simple in-plane rotation of the cation rings (4 structures; <1 kJ/mol difference) and three structures above 35 kJ/mol have not been included in the present analysis.

Results and Discussion

QTAIM molecular graphs and NCI isosurface plots of the IP-dimer structures are provided in **Figure 4**. The related BCP (ρ_b , $\nabla^2\rho_b$ and H_b) and $E^{(2)}$ data are listed in **Table 1**. On forming the IP-dimers there is an increase in the number of 1° and 2° interactions, and new π⁺-π⁺ interactions are observed. H-bonding and anion-π⁺ interactions can be evaluated through QTAIM and NBO analysis and via NCI isosurface plots. □

classification of doubly ionic H-bonds strengths, within ILs, based on QTAIM and NBO data has been recently proposed.⁵⁶ The criteria for strong ($\square\rho_b > 0.05$ au; $E^{(2)} > 150$ kJ/mol), medium (ρ_b 0.02-0.05 au; $E^{(2)}$ 30-150 kJ/mol) and weak (ρ_b 0.002-0.02 au; $E^{(2)} < 30$ kJ/mol) H-bonds are applied here.

$\pi^+-\pi^+$ stacked IP-dimers

Low-energy M_FS_SF_A (0.0 kJ/mol) and M_FS_SF_R (0.42 kJ/mol) exhibit parallel-displaced and stacked $\pi^+-\pi^+$ interactions together with out-of-plane front and side H-bonding interactions with the anions. These structures are consistent with $\pi-\pi$ structural arrangements observed for benzene dimers, i.e. stacked, T-shape and parallel displaced. The structures can be rationalised by the attractive arrangements of the quadrupole moments associated with the aromatic ring. In addition to electrostatic interactions, dispersion interactions affect preferential $\pi-\pi$ arrangements.^{3,25}

Coulombic repulsion between π -rings in a benzene dimer leads to a parallel-displaced structure.⁵³ The M_FS_SF_A IP-dimers exhibit a similar parallel-displaced structure. Higher energy conformers (≈ 4.1 kJ/mol) that exhibit parallel stacking are also found for benzene dimers,¹²⁶ and the M_FS_SF_R IP-dimer follows this kind of stacking conformation. However, compared to the benzene dimers, a significantly larger Coulombic repulsion is expected for the IP-dimers. The repulsive cationic charge on the π^+ rings must be stabilised by an attractive cation-anion (charge screening) interaction with the anions.

Results from both the QTAIM and NCIPLOT analysis indicate that weak $\pi^+-\pi^+$ dispersive interactions are present within these IP-dimers, **Figure 4**. QTAIM finds BCPs between atoms in the stacked rings, where small values of $\square\rho_b$ are indicative of dispersive interactions, Table 1. NCIPLOT surfaces of the IP-dimers show weak dispersive interactions (green surfaces, $\rho \approx \square\square\square \lambda_2 \approx 0$) similar to those shown previously for the benzene dimer.¹¹⁷

The qualitative QTAIM results and NCI isosurface plots do not precisely quantify the energy contributions from the Coulomb and dispersive contributions, however a symmetry-adapted perturbation theory analysis of a pyridinium bromide system provides supporting evidence for a large electrostatic contribution (≈ 80 -90 kJ/mol) further stabilised by a substantial dispersion component (≈ 40 -50 kJ/mol) in stacked IP-dimer structures.²⁷

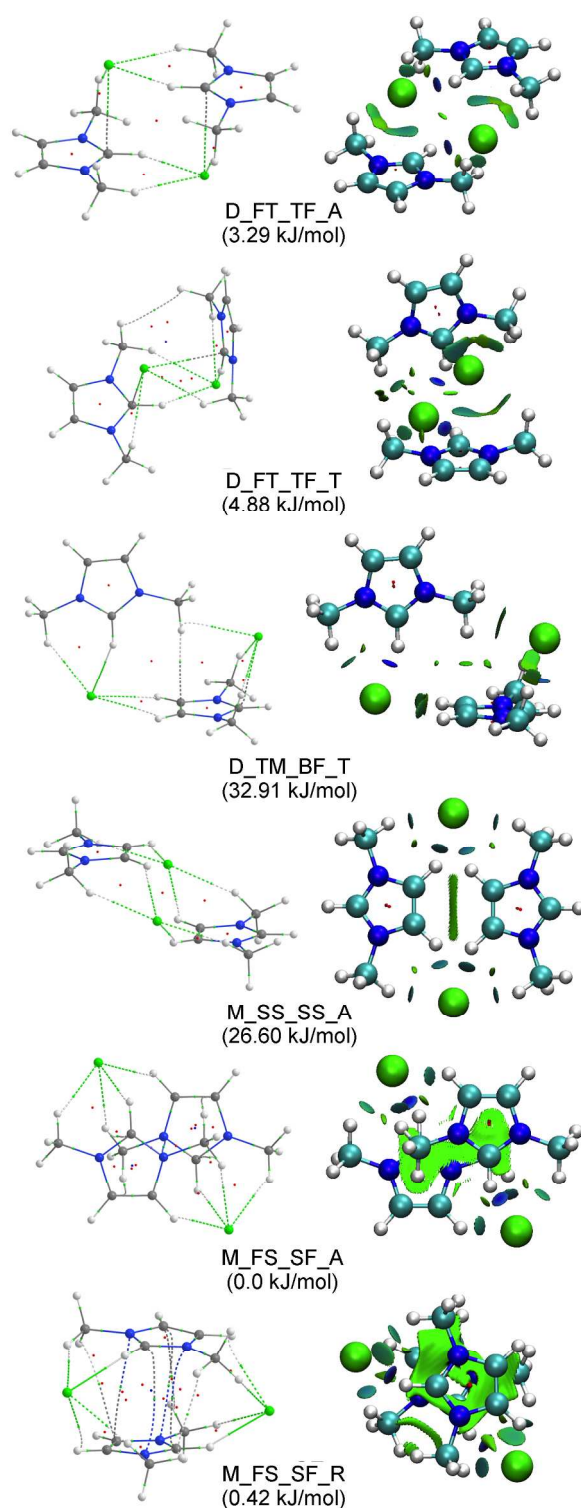
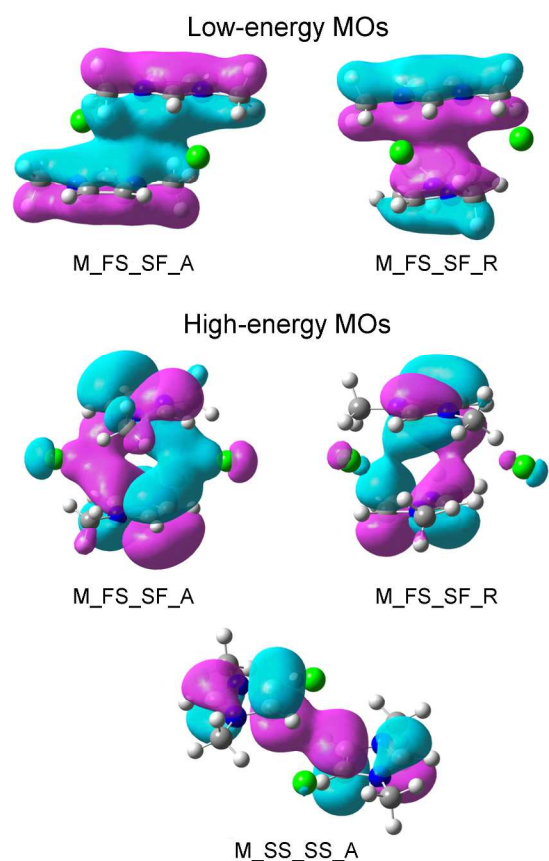


Figure 4. QTAIM molecular graphs and NCI isosurface plots for the $[C_1C_1im]_2Cl_2$ IP dimer conformers. Lines connecting the nuclei are the bond paths traced within the electron density distribution. The small dots indicate the positions of the BCPs (green) and RCPs (red). NCI isosurface plots are coloured via the strength of the interaction, blue (strong attractive), green (weak, VdW) and red (repulsive).

Table 1. Selected QTAIM and NBO data for the D_FT_TF_A and D_FT_TF_T [C₁C₁im]₂Cl₂ IP dimers

		ρ_b (au)	$\nabla\rho_b$ (au)	H _b (au)	$\Sigma E^{(2)}$ (kJ/mol)
D_FT_TF_A	F1°	0.025	0.062	0.000	58.4
	F2°	0.012	0.035	0.001	14.3
	T1°	0.014	0.038	0.001	40.5
	T2°	0.009	0.028	0.001	4.7
D_FT_TF_T	F1°	0.024	0.061	0.000	53.3
	F2°	0.012	0.034	-0.001	13.5
	T1°	0.015	0.039	-0.001	22.7
	T2°	0.009	0.029	-0.001	5.4
	H-H	0.002	0.008	-0.001	-
D_TM_BF_T Cation_1	F1°	0.033	0.071	-0.003	99.1
	F2°	0.013	0.037	0.001	16.3
	H- π	0.004	0.012	0.001	1.7
	Meth	0.011	0.037	0.002	9.1
	T1°	0.022	0.054	0.000	48.6
D_TM_BF_T Cation_2	T2°	0.007	0.022	0.001	16.3
	T2°	0.007	0.022	0.001	16.3
	B1°	0.009	0.030	0.001	3.6
	B1°	0.009	0.030	0.001	3.6
M_SS_SS_A	S1°	0.016	0.047	0.001	21.8
	S2°	0.017	0.047	0.001	25.2
M_FS_SF_A	F1°	0.023	0.064	0.001	39.9
	F2°	0.013	0.036	0.001	13.6
	S1°	0.014	0.042	0.001	14.9
	S2°	0.016	0.044	0.001	23.9
	$\pi^+(C2)-\pi^+(M)$	0.004	0.017	0.001	1.1
	$\pi^+(C4)-\pi^+(M)$	0.004	0.015	0.001	1.1
	$\pi^+(N)-\pi^+(N)$	0.003	0.013	0.001	-
	F1°	0.026	0.066	-0.001	61.4
	F2°	0.014	0.038	0.001	16.8
M_FS_SF_R	S1°	0.012	0.037	0.001	6.0
	S2°	0.016	0.043	0.001	20.3
	$\pi^+(C4)-\pi^+(M)$	0.003	0.009	0.001	-
	$\pi^+(C4)-\pi^+(N)$	0.003	0.010	0.001	0.9
	$\pi^+(C2)-\pi^+(N)$	0.004	0.013	0.001	0.9
	H-H	0.003	0.010	0.001	-

**Figure 5.** Representative lower- and higher-energy π -type interaction MOs for [C₁C₁im]₂Cl₂ IPs-dimers exhibiting $\pi^+-\pi^+$ interactions.

π -type MOs indicative of π - π interactions are also observed for the M_FS_SF_A and M_FS_SF_R IP-dimers (**Figure 5**). Moreover, a high-energy π -type MO has been found for the M_SS_SS_A conformer, showing overlap (interaction) between the C⁴=C⁵ double bond regions of each [C₁C₁im]⁺ ring (**Figure 5**). These results reinforce the existence of dispersion interactions between the [C₁C₁im]⁺ rings as observed in the NCI isosurface plots of **Figure 4**.

H-bonding and anion- π^+ interactions in the IP conformers

QTAIM molecular graphs and NCI isosurface plots for the front, side, back (H-bonding) and top (H-bonding and anion- π^+) IP conformers are presented in **Figure 6**. **Table 2** lists data for the H-bond (F1°, F2°, S1°, S2°, B1° and T2°) and anion- π^+ (T1°) interactions. ρ_b and $E^{(2)}$ indicate that the 1° H-bonding interactions for the front and side interactions are strong/medium and the 2° H-bonding interactions are medium/weak, whereas the 1° H-bonding interactions in the back conformer are both weak.

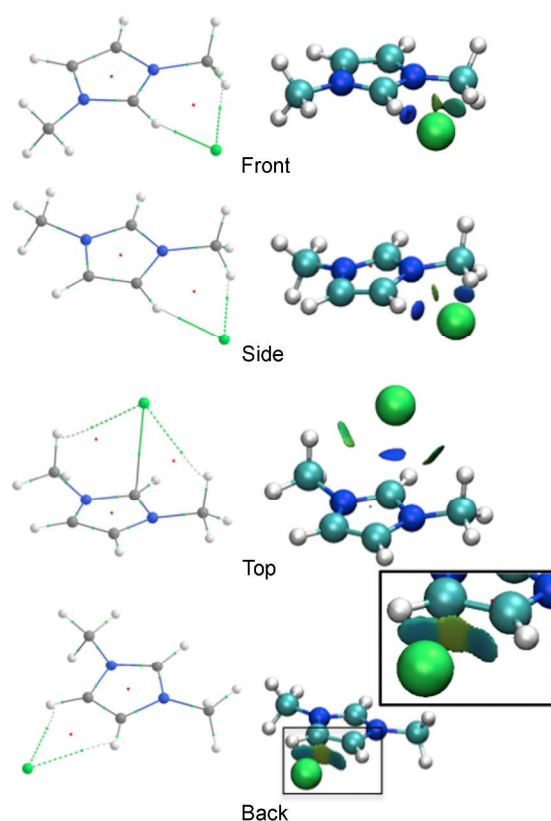


Figure 6. QTAIM molecular graphs and NCI isosurface plots for the $[C_4C_1im]Cl$ IP conformers. Lines connecting the nuclei are the bond paths traced within the electron density distribution. The small dots indicate the positions of the BCPs (green) and RCPs (red). NCI surfaces are coloured via the strength of the interaction, blue (strong attractive), green (weak, VdW) and red (repulsive).

Table 2. Selected QTAIM and NBO data for the $[C_4C_1im]Cl$ IPs

	ρ_b (au)	$\nabla^2\rho_b$ (au)	H_b (au)	$\Sigma E^{(2)}$ (kJ/mol)
F1°	0.046	0.072	-0.009	169.74
F2°	0.013	0.037	0.001	16.02
S1°	0.032	0.071	-0.003	84.98
S2°	0.023	0.057	0.000	44.48
B1°	0.016	0.050	0.002	11.80
B1°	0.016	0.050	0.002	11.84
T1°	0.032	0.065	-0.002	110.62
T2°	0.009	0.027	0.001	3.64
T2°	0.009	0.027	0.001	3.64

For the IP structures; in the front conformer the 2° interaction is $\approx 10\%$ of the primary interaction. In the top conformer the T1° anion- π^+ interaction is found to dominate the T2° interactions, which sum to $\approx 5\%$ of T1°. However, for the side conformer the 2° interaction is $\approx 50\%$ of the primary interaction. This result is consistent with vibrational data obtained for $[C_4C_1im]Cl$ IPs.⁷⁴ Moreover, the qualitative NCI isosurface plots show distinct differences between the 1° (dark blue) and 2° (light blue/green) interactions. Thus, for the front or top conformers one component of the chelating H-bond or

anion- π^+ interaction is almost entirely dominant, while for the side conformer the strength of the H-bonds is more evenly distributed.

H-bonding in the low energy (0-5 kJ/mol) IP-dimers

The Coulombic and $\pi^+-\pi^+$ interactions within M_FS_SF_A and M_FS_SF_R are supported by H-bonding between the cations and anions; primarily front and side (F1°, F2°, S1° and S2°) H-bonds. In contrast to the IPs, where the anion lies roughly in-plane with the ring, the anions are positioned on the periphery and between the two aromatic rings in these IP-dimers. This leads to strongly bent primary H-bonds which have a reduced strength, as determined by ρ_b and $E^{(2)}$, relative to the in-plane IP H-bonds. For example, the front C²H...Cl⁻ (F1°) angle is reduced from 179.9° ($\rho_b=0.046$ au) in the IP to 129.0° ($\rho_b=0.023$ au) and 145.2° ($\rho_b=0.026$ au) in M_FS_SF_A and M_FS_SF_R respectively. Proportionally S1° (C^{4/5}-H) interactions are reduced significantly more than F1° (C²-H) interactions. For example, in M_FS_SF_R S1° is $\approx 1/10$ and F1° is $\approx 1/3$ of the corresponding IP values. A stronger F1° interaction occurs in M_FS_SF_R, which is due to a slight tilting of the rings, associated with a further weakening of the S1° interaction.

A comparison of ρ_b and $E^{(2)}$ for the secondary H-bonds, shows that the front (F2°) interactions remain essentially identical on moving from the IP to the IP-dimers. Moreover, in the IPs the primary S1° is stronger than the secondary S2° (C^MH...Cl⁻) interactions. However, in the middle IP-dimers the methyl interactions are now stronger than the ring H-bonds. For example, the ratio of $E^{(2)}$ values within M_FS_SF_A and M_FS_SF_R are S2°/S1° ≈ 1.6 and ≈ 3.4 , respectively. This switch in H-bond strength is attributed to the ability of the methyl groups to rotate, resulting in linear C^MH...Cl⁻ H-bonds and suggests that secondary interactions could play a more significant role than initially anticipated. Nevertheless, the stronger S2° interactions are still reduced to $\approx 50\%$ that of the side interactions in the IPs.

On forming the D_FT_TF_A and D_FT_TF_T IP-dimers a significant decrease in $\square\rho_b$ and $E^{(2)}$ is found for several of the H-bonding interactions, as well as for the T1° anion- π^+ interaction. In contrast, $\square\rho_b$ and $\Sigma E^{(2)}$ for the 2° H-bonding interactions remain approximately the same as in the IPs. Thus, the stronger H-bonds and anion- π^+ interactions are sensitive to ion clustering, while the secondary H-bonding interactions remain relatively unaffected.

For example, in the D_FT_TF_A conformer each Cl⁻ is in a top and front position, and a significant decrease in the $\Sigma E^{(2)}$ values to $\approx 1/3$ of the relevant IP conformers is observed for the primary front and top interactions (F1° and T1°). In addition a $\approx 50\%$ decrease in $\square\rho_b$ is observed for these interactions and a decrease in interaction strength is indicated by the NCI isosurface plots (visualised by the colour change from dark to

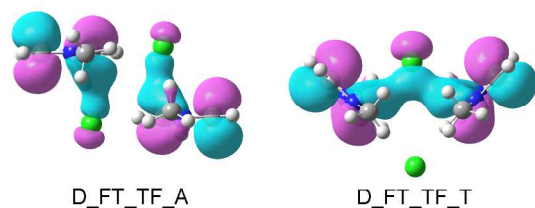


Figure 7. Representative higher energy π -type interaction MOs for $[\text{C}_1\text{C}_1\text{im}]_2\text{Cl}_2$ IP-dimers exhibiting anion- π^+ interactions.

light blue on moving from the IPs to the IP-dimers (ESI, Figure S1).

In D_FT_TF_T, where each Cl^- anion interacts via either a top-top or front-front position, the F1° interactions are $\approx 1/3$ while the T1° are $\approx 1/5$ that of the IPs. This indicates that the front interaction remains dominant whereas the top interaction weakens significantly in the IP-dimers. This decrease appears to be distance dependent; an increase of $\approx 0.3 \text{ \AA}$ is observed for both F1° and T1° on moving from the IP to the IP-dimer.

Figure 7 shows MOs which further emphasise the anion- π^+ character within these IP-dimers, and highlight the symmetric nature of these interactions.

Distance dependence in the H-bonding and anion- π^+ interactions

In order to further examine the distance dependence of the 1° and 2° interactions, and to contrast the front and top interactions, a distance scan between the Cl^- and $[\text{C}_1\text{C}_1\text{im}]^+$, in the front and top IP conformers, has been carried out. A scan of 20 steps of 0.05 \AA , followed by 20 steps of 0.1 \AA has been undertaken and $\square\rho_b$ computed at each point.

Plots of $\square\rho_b$ for the 1° (H-bonding and anion- π^+) and 2° (H-bonding) interactions are presented for the front conformer (starting at a $\text{C}^2\text{-Cl}^-$ distance of 3 \AA), Figure 8a, and for the top conformer, Figure 8b, (starting at a $\text{C}^2\text{-Cl}^-$ distance of 2.6 \AA). Each plot shows an exponential relationship between the $\text{CH}\cdots\text{Cl}^-$ and $\text{C}^2\cdots\text{Cl}^-$ distances and $\square\rho_b$. ρ_b is observed to decrease sharply for F1° and T1° H-bonding and anion- π^+ interactions, whereas a lesser distance dependence is observed for the 2° H-bond interactions, in both conformers. Furthermore, the decreased difference between 1° and 2° $\square\rho_b$ and H-bond strength, on moving from the IPs to the IP-dimers, values is clearly visualised.

The covalent character of a H-bond (at a BCP) may be characterised via the virial theorem⁷⁸

$$\left(\frac{1}{4}\right)\nabla^2 p_b = 2G_b + V_b$$

and H_b ,¹²⁷

$$H_b = V_b + G_b$$

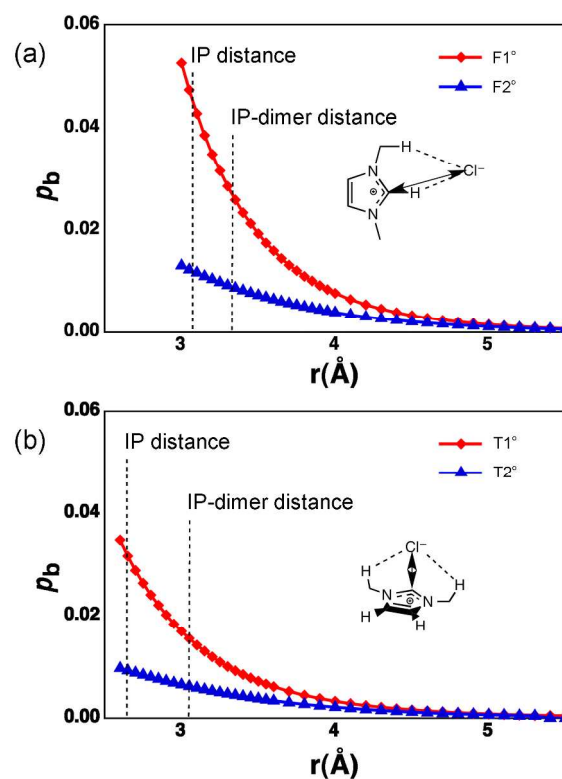


Figure 8. Plots of ρ_b for (a) the 1° (red) and 2° (blue) front H-bonding and (b) 1° A- π^+ -D and 2° top H-bonding interactions as a function of distance (r). The IP and IP-dimer distance labels indicate representative distances.

employing $\nabla\rho_b$, H_b and $(-V_b/G_b)$,¹²⁸ such that certain criteria are met; covalent bonds ($\nabla\rho_b < 0$, $H_b < 0$, $-V_b/G_b > 2$), partially covalent ($\nabla\rho_b < 0$ or $\nabla\rho_b > 0$, $H_b < 0$, $1 < -V_b/G_b > 2$)¹²⁹ and weak closed-shell, electrostatic interactions ($\nabla\rho_b > 0$, $H_b > 0$, $-V_b/G_b < 1$).

Plots of H_b and $-V_b/G_b$ against distance for the 1° and 2° interactions are provided in the ESI (Figure S2). $\nabla\rho_b > 0$ for each point along the scans, therefore employing the above criteria F1° and T1° interactions are classified as having partial covalent character over short-range distances up to $\approx 3.5 \text{ \AA}$ and $\approx 3.0 \text{ \AA}$ respectively. Beyond this distance the primary interactions are purely closed-shell, electrostatic interactions. Moreover, the 2° H-bond interactions (F2° and T2°) are classified as electrostatic.

In summary, 1° H-bond and anion- π^+ interactions have significant distance dependence and possess partially covalent and electrostatic character, whereas the 2° H-bonds represent purely closed-shell, electrostatic interactions. Moreover, the rapid decline of the primary interactions, leads to the weaker 2° H-bonds becoming more prominent on IP-dimer formation. We speculate that application of this conclusion to larger neutral clusters may result in an increased structuring role for the 2° H-bonds and less pronounced 1° H-bonding and anion- π^+ interactions.

Comparison of the low-energy (0-5 kJ/mol) IP-dimer conformers

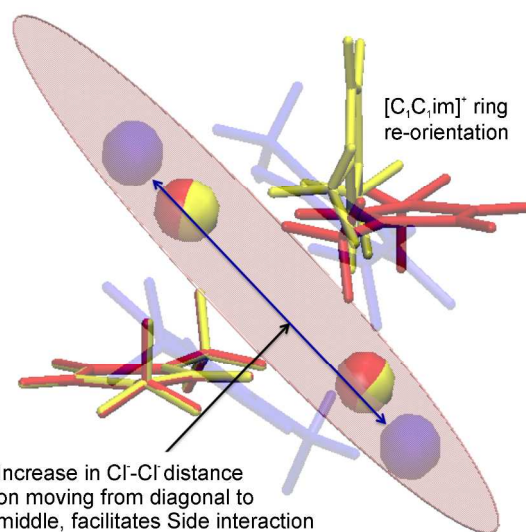


Figure 9. Overlay of optimised iso-energetic structures; D_FT_TF_A (red), D_FT_TF_T (yellow) and M_FS_SF_R (blue) IP-dimer conformers, employing the Cl⁻ anions as reference.

Figure 9 shows an overlay of the low-energy middle (M_FS_SF_R) and diagonal (D_FT_TF_A and D_FT_TF_T) conformers such that the Cl⁻ anions are in the same plane. The existence of these low-energy, iso-energetic but very structurally different conformers, indicates that large conformational differences can occur for very little cost in energy. For example, the energy barrier on moving from M_FS_SF_A to D_FT_TF_A has been previously determined to be ≈ 6 kJ/mol.⁵³ The energy barrier between D_FT_TF_T and D_FT_TF_A has been computed here to be ≈ 7.5 kJ/mol (ESI – **Figure S3**). Therefore, the essentially identical energy of the middle and diagonal structures indicates that charge screening is relatively independent of the precise orientation of the cation rings.

The main structural difference between the diagonal and middle structures is the exchange of a top (anion- π^+) with a side (H-bonding) interaction. The diagonal structures are associated with a very strong T1^o (anion- π^+) and very weak T2^o (methyl H-bonding) interaction, whereas, the middle structure is associated with slightly stronger S2^o (methyl) than S1^o (ring) H-bonding interactions. In terms of charge screening, the structural arrangement of the low-energy IP-dimer conformers forms a highly stable gas-phase arrangement that resembles a charge quadrupole. As such, charge screening in terms of an intuitive alternation of charge, cation-anion-cation-anion, will not be the most stable conformation for the IP-dimers.¹³⁰ However, in the middle IP-dimers charge screening can still occur with the anions positioned on the periphery of the cationic rings, allowing the aromatic rings to interact directly, **Figure 1**.

H-bonding in the medium energy IP-dimers

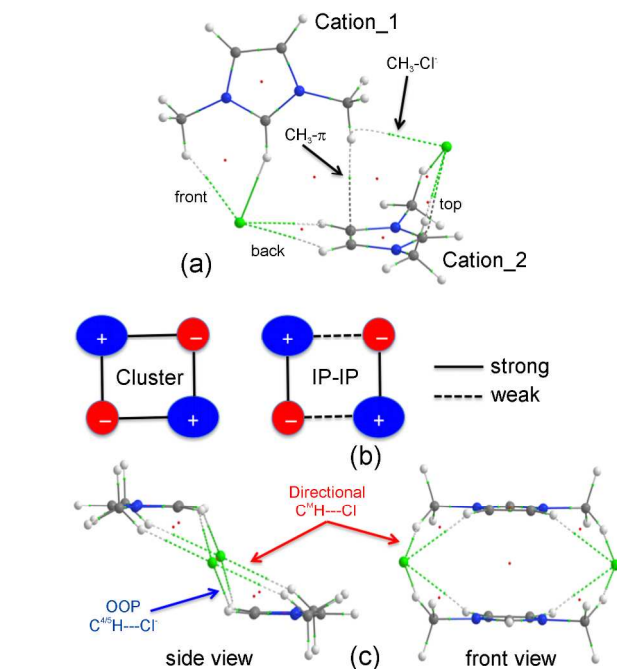


Figure 10. (a) D_TM_BF_T IP-dimer representing cation_1 and cation_2 that are in different chemical environments. (b) Cartoon of the cluster vs. IP-IP makeup of the D_FT_TF_A/D_FT_TF_R and D_TM_BT_T conformers and (c) side and front view of the M_SS_SS_A conformer with out-of-plane H-bonds (C⁴/H---Cl) and directional 2° C^{4M}/H---Cl H-bonds.

In contrast to the other IP-dimers (which have symmetrically related ions), each cation and each anion in the medium-energy D_TM_BF_T conformer (33 kJ/mol) is found in a different chemical environment (**Figure 10a**). Hence, data related to each individual cation is reported for D_TM_BF_T in **Table 1**. This conformer is also unique with respect to the others studied in that the structure appears to be composed of two IPs, which are loosely interacting (**Figure 10b**). The other IP-dimers have a more distinctive cluster like organisation with each cation interacting with both anions equally and vice versa.

The loose IP-IP association is evidenced in the $\square\rho_b$ and E⁽²⁾ H-bonding and anion- π^+ interactions. In the cluster like conformers the primary interactions are $\approx 1/3$ the IP interactions, however in D_TM_BF_T the primary interactions are much stronger, for example the F1^o interactions maintain $\approx 2/3$ the strength of the front IP conformer, and T1^o is $\approx 1/2$ that of the top IP. This is consistent with the generally shorter H-bond and anion- π^+ distances found for D_TM_BF_T. In contrast the 2° H-bonds are, like the clusters, $\approx 1/2$ those found in the IP conformers. Thus, in D_TM_BF_T, only the relatively weak B1^o and 2° (meth and CH₃- π) interactions are holding the two "IP-like" components together.

In the M_SS_SS_A conformer (26.6 kJ/mol) the [C₁C₁im]⁺ rings are displaced laterally relative to each other and the Cl⁻ anions are involved in multiple bent out-of-plane H-bonds, of a type not observed in the stable IP conformers (**Figure 10c**). This cluster is unexpectedly stable, given the weak out of plane H-bonds holding it together. The closest IP-conformers are

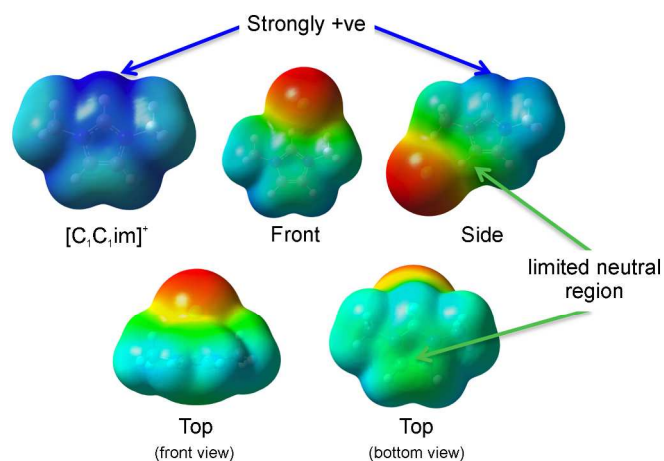


Figure 11: ESPs of the $[C_1C_1im]^+$ cation and selected $[C_1C_1im]Cl$ IPs. ESPs are generated on the 0.0004 au density isosurface. The surface colour scale is 0-1 au for the $[C_1C_1im]^+$ cation and ± 0.8 au for the IPs.

side-IP conformers, which are ≈ 30 kJ/mol above the more favourable front and top IP structures.

A comparison of ρ_b and $E^{(2)}$ for the bent H-bonding in $M_{SS_{SS}_A}$, relative to the side IP, reveals a significantly lower interaction strength for both $S1^\circ$ ($\approx 1/4$) and $S2^\circ$ ($\approx 1/2$). Nevertheless, the interaction with the ring and methyl H-atoms is essentially identical for both ρ_b and $E^{(2)}$. This is also re-enforced by a visual inspection of the NCI isosurface plots (**Figure 4**).

These results indicate that medium-energy IP-dimers (which may form in the condensed phase) can be composed of strong cation-anion IP and very weak linking interactions. Essentially these are loosely associated IP-IP structures. Moreover, medium-energy conformers can exhibit unconventional strongly out of plane H-bonding interactions, which are substantially stabilising.

Electrostatic potential surfaces for the IPs and IP-dimers

Coulomb forces are a driving structural feature of ILs. The $[C_1C_1im]^+$ cation is an electron-deficient, partially delocalised heteroaromatic ring. A plot of the ESP mapped onto a density isosurface for the $[C_1C_1im]^+$ cation (**Figure 11**) indicates regions of increased positive potential (dark blue) at which an interacting anion may favourably reside. These regions correspond to the front, side and top sites for anion location as indicated in **Figure 2**.

The number of observed positive regions (dark blue) are reduced on formation of the $[C_1C_1im]Cl$ IP conformers (**Figure 11**). For each conformer negative charge (red) is localised on the Cl^- , whereas the positive regions are now polarised opposite to the Cl^- position. In the front conformer this is to the back of the ring, in the side conformer this is to the front of the ring. In the top conformer the positive region now encompasses the ring (**Figure 11**; Top – front view) and a neutral region is formed below the ring (**Figure 11**; Top – bottom view).

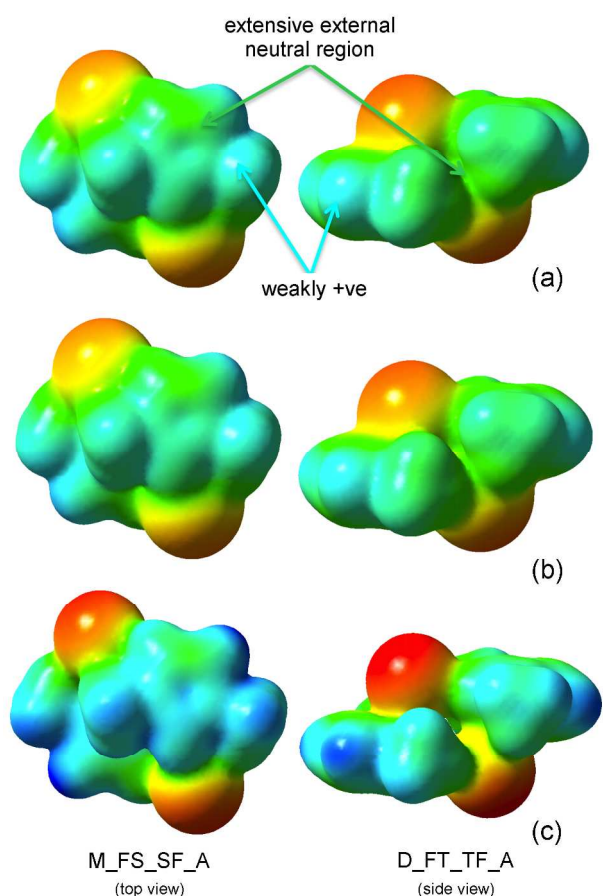


Figure 12: ESPs for the $M_{FS_{SF}_A}$ and $D_{FT_{TF}_A}$ IP-dimers conformers generated on the (a) 0.0004 au, (b) 0.001 au and (c) 0.004 au density isosurfaces. The surface colour scale is ± 0.8 au.

Table 3: Charge transfer from the Cl^- to the $[C_1C_1im]^+$ in the IPs and the sum of charge transfer from the Cl^- anions to the $[C_1C_1im]^+$ in the $[C_1C_1im]_2Cl_2$ IP-Dimers for each charge partitioning scheme. Average CT is calculated over all conformers.

	CHelpG	NBO	QTAIM
	IPs		
Front	0.262	0.158	0.154
Top	0.298	0.177	0.210
Side	0.228	0.128	0.139
Back	0.158	0.065	0.097
	IP-Dimers		
M_FS_SF_A	0.522	0.229	0.325
M_FS_SF_R	0.524	0.239	0.320
D_FT_TF_A	0.493	0.205	0.318
D_FT_TF_T	0.508	0.208	0.322
M_SS_SS_A	0.444	0.197	0.302
D_TM_BF_T	0.487	0.221	0.318

Visualisation of the $M_{FS_{SF}_A}$ and $D_{FT_{TF}_A}$ IP-dimer ESP isosurfaces at 0.0004au (**Figure 12a**) reveals a reduction in regions of large positive (dark blue) and large

negative (red) charge. The IP-dimers are charge screened relative to the IPs. **Figure 12 b and c** show the ESP mapped onto density isosurfaces at 0.001au and 0.004au respectively.

Further comparison of ESPs on isosurfaces of increasing density for each of the IP-dimer is provided in the **ESI, Figure S4**. Extensive neutral regions are evident on the exterior (diffuse) 0.0004 au density isosurface. Highly positive and negative regions of charge are buried within the electron cloud of the cluster, as indicated by ESP mapped onto the 0.004 au density isosurface.

Charges and charge transfer

A plot comparing individual Cl^- NBO charges for the IP-dimers is presented in **Figure 13**. A complete atomic list of NBO charges for each IP and IP-dimer is provided in the **ESI, Tables S1-S2**. Identical charges have been obtained for Cl^- anions resident in identical chemical environments, (M_FS_SF_A, M_FS_SF_R, M_SS_SS_A and D_FT_TF_A) whereas, Cl^- anions in different chemical environments, D_FT_TF_T and D_TM_BF_T, have small differences of 0.05e and 0.02e respectively.

Charge transfer (CT) from a Cl^- anion into a $[\text{C}_1\text{C}_1\text{im}]^+$ ring and subsequent polarisation of the cation may account in part for the electrostatic stabilisation on forming $[\text{C}_1\text{C}_1\text{im}]_2\text{Cl}_2$ IP-dimers. CT into the $[\text{C}_1\text{C}_1\text{im}]^+$ rings reduces the cation-anion Coulomb attraction, and potentially also leads to the simultaneous reduction of the Coulomb repulsion between ions with the same charge. This is evidenced by the reduced distances between the π^+ cation rings (≈ 3.4 Å) for the middle conformers, with the anions on the periphery too far apart (≈ 7 Å) to interact (**Figure 14**). In the diagonal conformers the reduction in Coulomb repulsion facilitates both anion-anion (≈ 4 Å apart) and cation-cation close contact.

Total CT, from the Cl^- anion(s) to the $[\text{C}_1\text{C}_1\text{im}]^+$ cation(s) for the IP and IP-dimers has been determined using each of the CHelpG, NBO and QTAIM partitioning schemes, **Table 3**. In general, only a small variation in CT is observed between different IP-dimers. CT is found to be non-additive on moving from IPs to the IP-dimers. For example, each Cl^- in D_FT_TF_A has CT of 0.103e, which is less than the CT found in the front (0.158e) and top (0.177e) IPs, for the NBO charges. The reduction in CT may, in part, be due to an increased cation-anion distance in the IP-dimers.

On moving from IPs to IP-dimers, NBO predicts a net decrease of $\approx 0.02\text{e}$ in CT per Cl^- (IP=0.132e; IP-dimer=0.108e) averaged for each of the conformers. In contrast, both CHelpG (IP=0.237e; IP-dimer=0.248e) and QTAIM (IP=0.150e; IP-dimer=0.159e) indicate a net increase of CT $\approx 0.01\text{e}$ per Cl^- . The small difference in average CT between IPs and IP-dimers suggests that averaged IPs CT (at reduced computational cost) may be sufficient for use in the parameterisation of MD force fields. Therefore, the choice of charge partitioning scheme used to obtain CT is extremely important. The smaller CT obtained using the NBO scheme, is consistent with recent MD results, wherein the inclusion of polarisation resulted in a reduced CT of $\approx 0.03\text{e}$, in the condensed phase.¹³¹

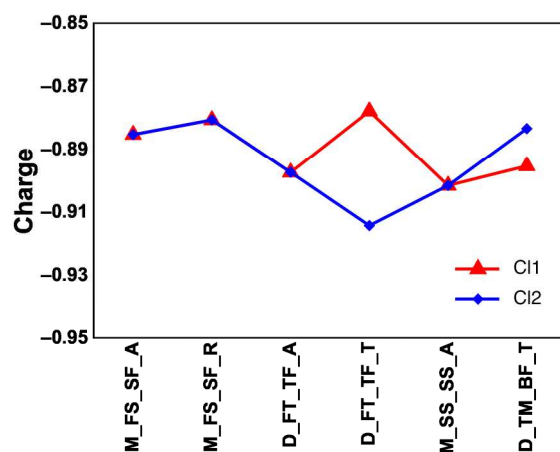


Figure 13. Plot of the Cl^- charges, obtained from NBO analysis, for each Cl^- per IP-dimer. IP-dimers are arranged from lowest to highest relative energy.

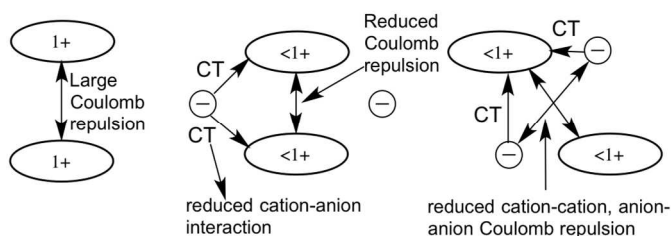


Figure 14: Cartoon representing reduction of cation-cation Coulomb interactions and charge transfer for an example middle IP-dimer. A reduction of anion-anion Coulomb interactions also occurs in the diagonal IP-dimers.

In order to examine the movement of electron density on the formation of an IP, electron density difference maps have been generated for the front, top and side structures (**Figure 15**). For the front IP, electron density has shifted away from the H-atom and into the inter-nuclear $\text{H}\cdots\text{Cl}^-$ region, while the C^2 atom has gained electron density. Similar effects have been reported recently for $[\text{C}_2\text{C}_1\text{im}][\text{NTf}_2]$ and $[\text{C}_2\text{C}_1\text{im}][\text{OAc}]$ IPs.^{132,133} The side structure shows electron density movement into the inter-nuclear $\text{H}\cdots\text{Cl}^-$ region for both ring and methyl protons. For the top IP, there is a decrease in the electron density over the N- C^2 -N atoms at the front of the ring and an increase in electron density in the $\text{C}^2\cdots\text{Cl}^-$ inter-nuclear region. Therefore, the density difference plots show that polarisation is not restricted to specific atoms, but includes the whole molecule. It is anticipated that polarisation is stabilising the IPs and IP-dimers through changing internal and IP Coulombic interactions.

In summary, evidence has been provided indicating that charge polarisation occurs over the entire $[\text{C}_1\text{C}_1\text{im}]^+$ ring, rather than being localised on forming H-bonding and anion- π^+ interactions. Moreover, CT is found to be similar for disparate IP-dimer structural motifs and extensive neutral outer regions contrast with highly polarised interiors.

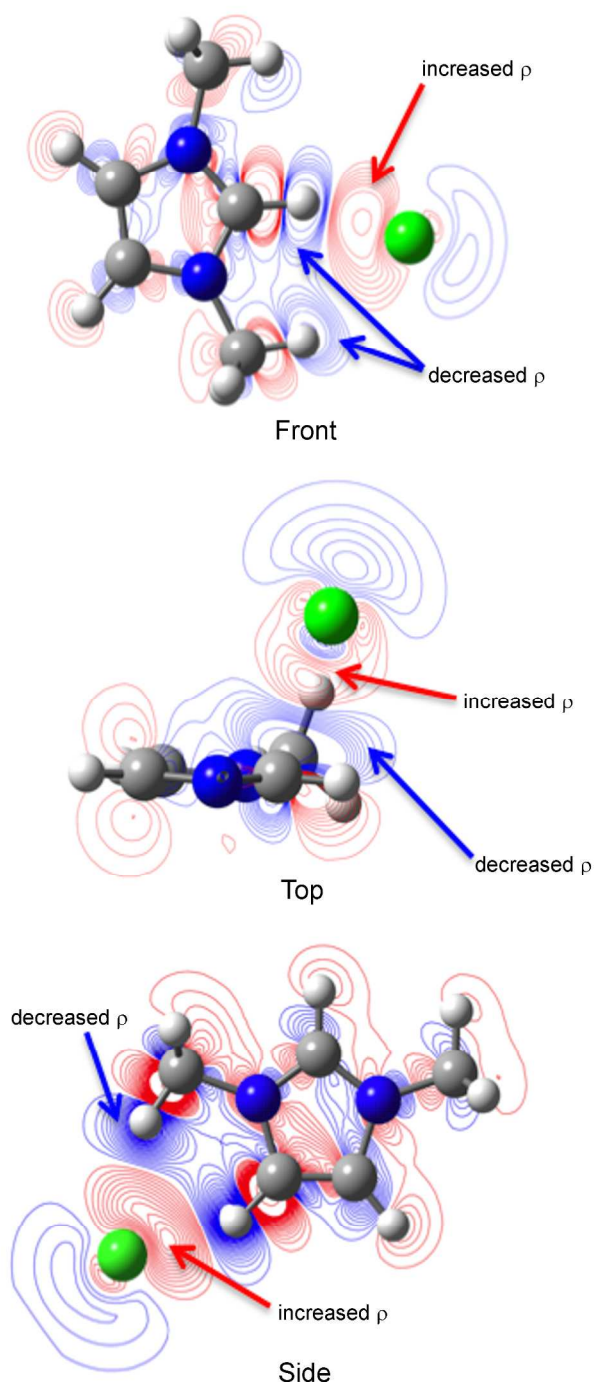


Figure 15. Electron density difference maps for the formation of $[C_1C_1im]Cl$ front, top and side IP conformers. A methyl substituent in the top conformer has been removed for clarity. Blue=reduction and red=increase in electron density relative to the isolated ions. Contours at density intervals of 0.0005 (0-0.01), 0.01 (0.01-0.1), 0.1 (0.1-1) and 2, 4, 8 and 20 au.

MOs of the IP-dimers

Qualitative MO analysis provides a descriptive tool for explaining chemical bonding. MOs are used to help explain H-bonding, anion- π^+ and $\pi^+-\pi^+$ interactions observed in the QTAIM and NBO analysis. The highest occupied molecular orbital (HOMO) region of the IP-dimers is composed of both

bonding and anti-bonding pairs of the anion highest occupied frontier orbitals (the HOF0, HOF0-1 and HOF0-2 which are the filled 3p AOs on the Cl^- ions.) together with bonding and anti-bonding pairs of the cation HOF0 and HOF0-1 (π anti-bonding MOs based on the ring). The HOMO for each of the IP-dimer conformers is primarily located on the anion, **Figure 16**. A unique through space anion-anion interaction is observed for the HOMO of the symmetric $D_{FT_TF_A}$ IP-dimer.

Representative low- and high-energy H-bond MOs are shown in **Figures 17-18**. Slightly more interaction is observed in the deeper, lower-energy H-bonding MOs (**Figure 17**). However, consistent with MOs determined for the IPs (**ESI, Figures S5-S6**) there is, in-general, very little delocalisation of the cation or anion MOs over the clusters.

Structures with ‘symmetric’ anion chemical environments have MOs composed of two localised FO contributions, with equal weighting, based primarily on the cation or the anion. For example, in the MOs of **Figure 18** contrast the equal but localised FOs on both Cl^- ions (and to a lesser extent the cations) for $M_{SS_SS_A}$ with the highly localised FO on a single Cl^- ion for $D_{TM_BF_T}$.

The diagonal $D_{FT_TF_T}$ and $D_{TM_BF_T}$ IP-dimers show enhanced localisation because the Cl^- anions reside in non-equivalent chemical environments. The $D_{FT_TF_T}$ conformer exhibits symmetric cation contributions but an asymmetric anion contribution leading to a top- Cl^- -top (**Figure 16**) and a front- Cl^- -front (**Figure 17**) interaction. The $D_{TM_BF_T}$ conformer exhibits unsymmetrical contributions for both the cation and anion supporting the representation of this conformer as two ‘associated’ IPs rather than as a cluster.

High-energy π -type MOs involving anion- π^+ interactions are shown for the $D_{FT_TF_A}$ and $D_{FT_TF_T}$ IP-dimers in **Figure 7**. The anion- π^+ interactions are highly directional and occur only with the $N^1-C^2-N^3$ moiety at the front of the $[C_1C_1im]^+$ ring. No lower energy anion- π^+ bonding MO interactions were identified for the diagonal conformers. However, deep low energy MOs are identified for the $M_{FS_SF_A}$ and $M_{FS_SF_R}$ IP-dimers (**Figure 5**).

In summary, the (localised) MO description of the IP-dimers reinforces the ionic nature of the inter-ion interactions. However, weaker covalent interactions as represented by delocalisation within the MOs are evident; key are the deep MOs that exhibit cation-anion H-bonding. Moreover, a number of MOs exhibit non-trivial anion-anion, anion- π^+ and cation-cation (π - π) interactions.

Conclusions

In this paper, we have examined $\pi^+-\pi^+$, H-bonding, and anion- π^+ interactions presented in $[C_1C_1im]Cl$ IPs and selected $[C_1C_1im]_2Cl_2$ IP-dimers. Methods of analysis included ESP and NCI isosurface plots, partial charges (NBO, CHelpG, AIM), density descriptors from QTAIM (ρ_B), the NBO energy parameter $E^{(2)}$ and qualitative MO analysis.

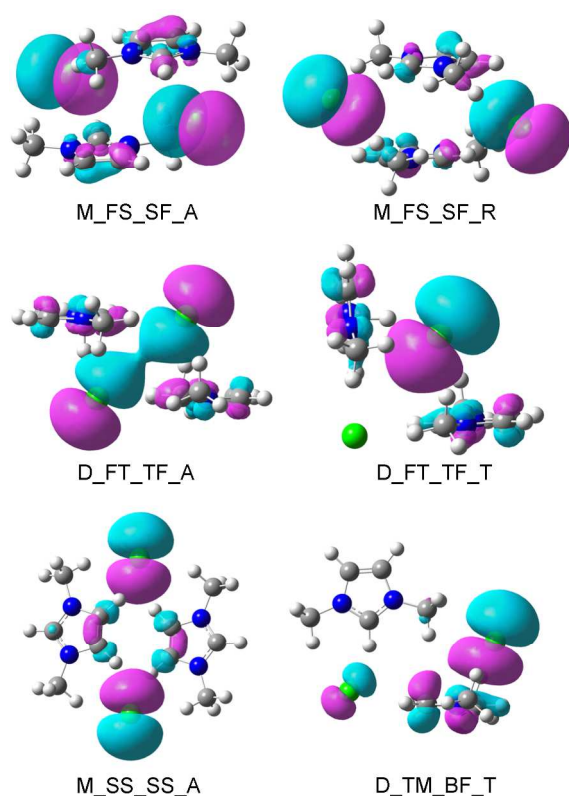


Figure 16. HOMOs of the essentially 'pure' Cl^- anion in the $[\text{C}_1\text{C}_1\text{im}]_2\text{Cl}_2$ IP-dimers.

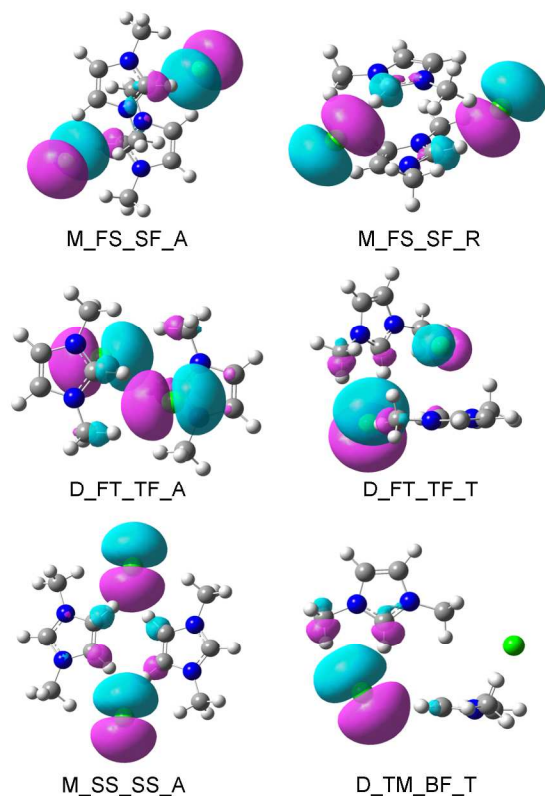


Figure 18. Representative high-energy H-bond interaction MOs for each of the $[\text{C}_1\text{C}_1\text{im}]_2\text{Cl}_2$ IPs-dimers.

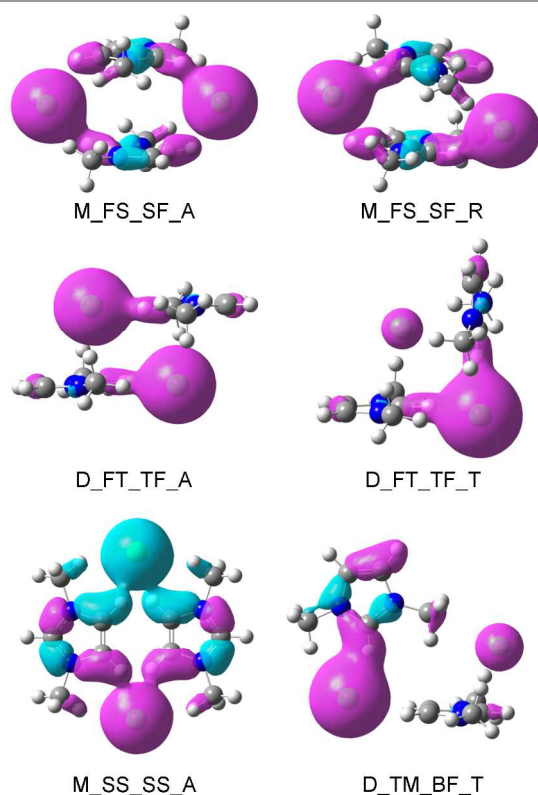


Figure 17. Representative lower-energy H-bond interaction MOs for each of the $[\text{C}_1\text{C}_1\text{im}]_2\text{Cl}_2$ IPs-dimers.

$\pi^+-\pi^+$ dispersive interactions are presented in the low-energy IP-dimers. The IP-dimers M_FS_SF_A and M_FS_SF_R exhibit parallel-displaced and stacked structures, analogous to benzene dimers. Cation-cation repulsion is reduced by anion charge screening, which appears insensitive to the orientation of the aromatic rings. \square QTAIM found BCPs between atoms of the stacked rings, NCI isosurface plots show weak dispersive interactions and π -type MOs indicative of π - π interactions have been found.

In the IP-dimers, the strength of the 1° H-bonding ($\text{C}^{2/4/5}\text{H}\cdots\text{Cl}^-$) and anion- π^+ ($\text{C}^2\cdots\text{Cl}^-$) interactions are classified as medium and the 2° H-bonds are weak. Primary and secondary interactions are found to be distance dependent and exhibit a general decrease in strength. However, it was found that primary interactions decrease more rapidly, than secondary interactions. This rapid decline of the primary interactions, leads to weaker 2° H-bonds becoming more prominent on IP-dimer formation, and results in a reversal of the 1° ring and 2° alkyl H-bond strengths in the IP-dimers that contain side IP motifs. Moreover, primary interactions exhibit partial covalent character over short distances and ionic character over longer distances, whereas secondary interactions exhibit only non-covalent (ionic and dispersive) character.

The medium-energy D_TM_BF_T conformer (32.9 kJ/mol) is found to be essentially composed of two loosely interacting IPs, whereas the other IP-dimers form ionic clusters. The M_SS_SS_A conformer (26.6 kJ/mol) exhibits unconventional

strongly bent out of plane H-bonding interactions, which are substantially stabilising.

Analysis of the IP-dimers has shown that subtle structural differences arise due to the array of medium to weak H-bonds, π^+ - π^+ -stacking and anion- π^+ interactions which can form. These interactions are able to fluctuate in strength, forming a small number of stronger interactions or a larger number of more moderate interactions for very little cost in energy. This is in contrast to biological systems and crystal engineering where π -stacking, anion- π and H-bonding impart a much stronger secondary structuring.

Comparison of the low-energy conformers has revealed that relatively large conformational changes, associated with exchange of top (diagonal) for side (middle) interactions, occur with little cost in energy. Viewed another way, the energy of the IP-dimer clusters is relatively independent of $[\text{C}_1\text{C}_1\text{im}]^+$ ring orientation. This reflects the non-specific Coulombic interactions that are driving the primary structuring of IP-dimers via charge screening. Efficient charge screening in the IP-dimers was validated via visualisation of the ESP, which revealed a highly polar interior, but extensive neutral regions externally. This is in contrast to the IPs, which are highly polarised and have exposed charge.

CT can also stabilise an IP-dimer reducing Coulombic interactions, however the absolute CT was found to be dependent on the partitioning scheme, i.e. NBO indicates a reduction in CT (more ionic), whereas, CHelpG and QTAIM show a slight increase in CT (less ionic). However, across the IP-dimers studied, CT per Cl^- varied only a small amount ($\pm 0.05e$) for each of the methods employed. Moreover, CT has been found to be non-additive (i.e. not an average of the CT of the two contributing IPs). Density difference maps show that CT (formation of the H-bond) results in charge reorganisation across the whole cation, and is not just local to the H-bond. CT is facilitated by orbital coupling, however, MOs remain highly localised, with deep MOs exhibiting slightly more delocalisation than high-energy MOs. H-bonding orbital interactions are evident.

In summary, CT and polarisation were found to stabilise $[\text{C}_1\text{C}_1\text{im}]_2\text{Cl}_2$ IP-dimer clusters. CT was found to be non-additive and polarisation was indicated over the $[\text{C}_1\text{C}_1\text{im}]^+$ ring rather than localised at cation-anion interaction sites. Moreover, the IP-dimer clusters form non-directional charge quadrupolar arrangements, but retain structural fluidity for both cation and anion, which allows for large conformational changes at little energy cost. This interchange is facilitated by the varying strengths of distant dependant primary and secondary H-bond interactions, coupled with anion- π^+ and π^+ - π^+ interactions. Both primary and secondary interactions decrease as a function of distance, however, decay of the primary interactions is more rapid. The convergence of the primary and secondary interactions strengths, and increased strength of secondary vs. primary H-bond interactions for the side IP conformer, indicates that secondary alkyl-chloride H-bonds may play a more significant role in structuring imidazolium chloride ILs and in its condensed phase chemistry.

Acknowledgements

R.P.M. acknowledges post-doctoral financial support provided through an *ERC Advanced Investigator Grant* held by Prof. Welton and Dr Hunt. Dr Kevin Lovelock is thanked for helpful discussion.

Notes and references

a Department of Chemistry, Imperial College London, London, SW7 2AZ, UK.

Email: richard.matthews@imperial.ac.uk; p.hunt@imperial.ac.uk

Electronic Supplementary Information (ESI) available: NCIPLOT isosurface plots indicating weakening of front and top IP primary interaction on forming an IP-dimer, plot of Hb, $-V_b/G_b$ and CT vs distance for 1° and 2° front and top interactions, ESPs for each of the IP-dimers at various isosurface values, scan of the energy barrier between D_FT_TF_T to D_FT_TF_A, tabulated lists of NBO partial atomic charges for each of the ion-pair and ion-pair dimer conformers, plot of the electron density difference maps for the side ion-pair structure and ion-pair low- and high-energy H-bond MOs.

See DOI: 10.1039/b000000x/

1. C. A. Hunter, J. Singh, and J. M. Thornton, *J. Mol. Biol.*, 1991, **218**, 837–846.
2. K. S. Kim, P. Tarakeshwar, and J. Y. Lee, *Chem. Rev.*, 2000, **100**, 4145–4186.
3. C. D. Sherrill, *Acc. Chem. Res.*, 2013, **46**, 1020–1028.
4. M. L. Waters, *Curr Opin Chem Biol*, 2002, **6**, 736–741.
5. M. Brandl, M. S. Weiss, A. Jabs, J. Sühnel, and R. Hilgenfeld, *J. Mol. Biol.*, 2001, **307**, 357–377.
6. O. Takahashi, Y. Kohno, and K. Saito, *Chem. Phys. Lett.*, 2003, **378**, 509–515.
7. B. Nepal and S. Scheiner, *J. Phys. Chem. A*, 2014, **118**, 9575–9587.
8. M. Nishio, Y. Umezawa, J. Fantini, M. S. Weiss, and P. Chakrabarti, *Phys. Chem. Chem. Phys.*, 2014, **16**, 12648–12683.
9. K. S. Kim, J. Y. Lee, S. J. Lee, T.-K. Ha, and D. H. Kim, *J. Am. Chem. Soc.*, 1994, **116**, 7399–7400.
10. D. A. Dougherty, *Science*, 1996, **271**, 163–168.
11. J. C. Ma and D. A. Dougherty, *Chem. Rev.*, 1997, **97**, 1303–1324.
12. A. S. Mahadevi and G. N. Sastry, *Chem. Rev.*, 2013, **113**, 2100–2138.
13. D. Quiñero, C. Garau, C. Rotger, and A. Frontera, *Angew. Chem. Int. Ed. Engl.*, 2002, 3539–3541.
14. B. L. Schottel, H. T. Chifotides, and K. R. Dunbar, *Chem. Soc. Rev.*, 2008, **37**, 68–83.
15. A. Frontera, P. Gamez, M. Mascal, T. J. Mooibroek, and J. Reedijk, *Angew. Chem. Int. Ed.*, 2011, **50**, 9564–9583.
16. P. de Hoog, P. Gamez, I. Mutikainen, U. Turpeinen, and J. Reedijk, *Angew. Chem.*, 2004, **116**, 5939–5941.
17. M. M. Watt, M. S. Collins, and D. W. Johnson, *Acc. Chem. Res.*, 2013, **46**, 955–966.
18. P. Kar, R. Biswas, M. G. B. Drew, A. Frontera, and A. Ghosh, *Inorg Chem*, 2012, **51**, 1837–1851.
19. S. Burley and G. Petsko, *Science*, 1985, **229**, 23–28.
20. J. Sponer, J. Leszczynski, and P. Hobza, *J. Biomol. Struct. Dyn.*, 1996, **14**, 117–135.
21. R. Bhattacharyya, U. Samanta, and P. Chakrabarti, *Protein Engineering Design and Selection*, 2002, **15**, 91–100.
22. V. Percec, M. Glodde, T. K. Bera, Y. Miura, I. Shiyonovskaya, K. D. Singer, V. S. K. Balagurusamy, P. A. Heiney, I. Schnell, A. Rapp, H.-W. Spiess, S. D. Hudson, and H. Duan, *Nature*, 2002, **419**, 384–387.
23. J. Cornil, D. Beljonne, J. P. Calbert, and J. L. Brédas, *Adv. Mater.*, 2001, **13**, 1053–1067.
24. L. Zang, Y. Che, and J. S. Moore, *Acc. Chem. Res.*, 2008, **41**, 1596–1608.
25. N. J. Singh, S. K. Min, D. Y. Kim, and K. S. Kim, *J. Chem. Theory Comput.*, 2009, **5**, 515–529.
26. S. K. Seth, P. Manna, N. J. Singh, M. Mitra, A. D. Jana, A. Das, S. R. Choudhury, T. Kar, S. Mukhopadhyay, and K. S. Kim, *Cryst. Eng.*, 2013, **15**, 1285–1288.

27. I. Geronimo, N. J. Singh, and K. S. Kim, *Phys. Chem. Chem. Phys.*, 2011, **13**, 11841–11845.
28. A. Das, A. D. Jana, S. K. Seth, B. Dey, S. R. Choudhury, T. Kar, S. Mukhopadhyay, N. J. Singh, I.-C. Hwang, and K. S. Kim, *J Phys Chem B*, 2010, **114**, 4166–4170.
29. P. Manna, S. K. Seth, M. Mitra, S. R. Choudhury, A. Bauzá, A. Frontera, and S. Mukhopadhyay, *Crystal Growth & Design*, 2014, 141007093122005.
30. K. Shimizu, M. F. Costa Gomes, A. A. H. Pádua, L. P. N. Rebelo, and J. N. Canongia Lopes, *J Phys Chem B*, 2009, **113**, 9894–9900.
31. T. Welton, *Chem. Rev.*, 1999, **99**, 2071–2084.
32. X. Zhang, X. Zhang, H. Dong, Z. Zhao, S. Zhang, and Y. Huang, *Energy Environ. Sci.*, 2012, **5**, 6668–6681.
33. R. P. Swatloski, S. K. Spear, J. D. Holbrey, and R. D. Rogers, *J. Am. Chem. Soc.*, 2002, **124**, 4974–4975.
34. A. Brandt, M. J. Ray, T. Q. To, D. J. Leak, R. J. Murphy, and T. Welton, *Green Chem.*, 2011, **13**, 2489–2499.
35. A. Brandt, J. Gräsvik, J. P. Hallett, and T. Welton, *Green Chem.*, 2013, **15**, 550–583.
36. P. Simon and Y. Gogotsi, *Nat. Mater.*, 2008, **7**, 845–854.
37. Y. Bai, Y. Cao, J. Zhang, M. Wang, R. Li, P. Wang, S. M. Zakeeruddin, and M. Grätzel, *Nat. Mater.*, 2008, **7**, 626–630.
38. M. Armand, F. Endres, D. R. MacFarlane, H. Ohno, and B. Scrosati, *Nat. Mater.*, 2009, **8**, 621–629.
39. A. Somers, P. Howlett, D. MacFarlane, and M. Forsyth, *Lubricants* 2013, Vol. 1, Pages 3-21, 2013, **1**, 3–21.
40. F. Zhou, Y. Liang, and W. Liu, *Chem. Soc. Rev.*, 2009, **38**, 2590–2599.
41. C. Ye, W. Liu, Y. Chen, and L. Yu, *Chem. Comm.*, 2001, 2244–2245.
42. S. Perkin, T. Albrecht, and J. Klein, *Phys. Chem. Chem. Phys.*, 2010, **12**, 1243–1247.
43. J. S. Wilkes and M. J. Zaworotko, *J. Chem. Soc., Chem. Comm.*, 1992, 965–967.
44. J. S. Wilkes and M. J. Zaworotko, *Supramolecular Chemistry*, 1993, **1**, 191–193.
45. M. Deetlefs, C. Hardacre, M. Nieuwenhuyzen, A. A. H. Pádua, O. Sheppard, and A. K. Soper, *J Phys Chem B*, 2006, **110**, 12055–12061.
46. M. Deetlefs, C. Hardacre, M. Nieuwenhuyzen, O. Sheppard, and A. K. Soper, *J Phys Chem B*, 2005, **109**, 1593–1598.
47. N. Dias, K. Shimizu, P. Morgado, E. J. M. Filipe, J. N. Canongia Lopes, and F. Vaca Chávez, *J Phys Chem B*, 2014, **118**, 5772–5780.
48. R. M. Lynden-Bell, L. Xue, G. Tamas, and E. L. Quitevis, *J. Chem. Phys.*, 2014, **141**, 044506.
49. B. Aoun, A. Goldbach, S. Kohara, J.-F. Wax, M. A. González, and M.-L. Saboungi, *J Phys Chem B*, 2010, **114**, 12623–12628.
50. J. de Andrade, E. S. Böes, and H. Stassen, *J Phys Chem B*, 2008, **112**, 8966–8974.
51. M. Brüssel, M. Brehm, A. S. Pensado, F. Malberg, M. Ramzan, A. Stark, and B. Kirchner, *Phys. Chem. Chem. Phys.*, 2012, **14**, 13204–13215.
52. H. Li, J. A. Boatz, and M. S. Gordon, *J. Am. Chem. Soc.*, 2008, **130**, 392–393.
53. R. P. Matthews, T. Welton, and P. A. Hunt, *Phys. Chem. Chem. Phys.*, 2014, **16**, 3238–3253.
54. E. Buisine, K. de Villiers, T. J. Egan, and C. Biot, *J. Am. Chem. Soc.*, 2006, **128**, 12122–12128.
55. R. P. Matthews, C. Ashworth, T. Welton, and P. A. Hunt, *J Phys Condens Matter*, 2014, **26**, 284112.
56. P. A. Hunt, C. R. Ashworth, and R. P. Matthews, *Chem. Soc. Rev.*, 2015, **44**, 1257–1288.
57. P. A. Hunt, B. Kirchner, and T. Welton, *Chem. Eur. J.*, 2006, **12**, 6762–6775.
58. P. A. Hunt, *J Phys Chem B*, 2007, **111**, 4844–4853.
59. E. I. Izgorodina, R. Maganti, V. Armel, P. M. Dean, J. M. Pringle, K. R. Seddon, and D. R. MacFarlane, *J Phys Chem B*, 2011, **115**, 14688–14697.
60. I. Skarmoutsos, D. Dellis, R. P. Matthews, T. Welton, and P. A. Hunt, *J Phys Chem B*, 2012, **116**, 4921–4933.
61. I. Skarmoutsos, T. Welton, and P. A. Hunt, *Phys. Chem. Chem. Phys.*, 2014, **16**, 3675.
62. R. Hayes, S. Imberti, G. G. Warr, and R. Atkin, *Angew. Chem. Int. Ed. Engl.*, 2013, **52**, 4623–4627.
63. A. G. Avent, P. A. Chaloner, M. P. Day, K. R. Seddon, and T. Welton, *J. Chem. Soc., Dalton Trans.*, 1994, 3405–3413.
64. K. Fumino, S. Reimann, and R. Ludwig, *Phys. Chem. Chem. Phys.*, 2014, **16**, 21903–21929.
65. M. Kohagen, M. Brehm, Y. Lingscheid, R. Giernoth, J. Sangoro, F. Kremer, S. Naumov, C. Jacob, J. Kärger, R. Valiullin, and B. Kirchner, *J Phys Chem B*, 2011, **115**, 15280–15288.
66. K. Wendler, J. Thar, S. Zahn, and B. Kirchner, *J. Phys. Chem. A*, 2010, **114**, 8.
67. D. Glas, J. Hulsbosch, P. Dubois, K. Binnemans, and D. E. De Vos, *ChemSusChem*, 2014, **7**, 610–617.
68. D. M. Phillips, L. F. Drummy, D. G. Conrady, D. M. Fox, R. R. Naik, M. O. Stone, P. C. Trulove, H. C. De Long, and R. A. Mantz, *J. Am. Chem. Soc.*, 2004, **126**, 14350–14351.
69. L. Cammarata, S. G. Kazarian, P. A. Salter, and T. Welton, *Phys. Chem. Chem. Phys.*, 2001, **3**, 5192–5200.
70. S. Zahn, K. Wendler, L. Delle Site, and B. Kirchner, *Phys. Chem. Chem. Phys.*, 2011, **13**, 15083–15093.
71. J. Le Bideau, L. Viau, and A. Vioux, *Chem. Soc. Rev.*, 2011, **40**, 907–925.
72. A. I. Horowitz and M. J. Panzer, *Angew. Chem. Int. Ed. Engl.*, 2014, **53**, 9780–9783.
73. J. Rigby and E. I. Izgorodina, *Phys. Chem. Chem. Phys.*, 2013, **15**, 1632–1646.
74. P. A. Hunt and I. R. Gould, *J. Phys. Chem. A*, 2006, **110**, 2269–2282.
75. S. Kossmann, J. Thar, B. Kirchner, P. A. Hunt, and T. Welton, *J. Chem. Phys.*, 2006, **124**, 174506.
76. E. Bodo, S. Mangialardo, F. Ramondo, F. Ceccacci, and P. Postorino, *J Phys Chem B*, 2012, **116**, 13878–13888.
77. K. Fumino, V. Fossog, K. Wittler, R. Hempelmann, and R. Ludwig, *Angew. Chem. Int. Ed. Engl.*, 2013, **52**, 2368–2372.
78. R. F. W. Bader, *Atoms in Molecules*, Oxford University Press, 1994.
79. R. F. W. Bader, *Chem. Rev.*, 1991, **91**, 893–928.
80. A. E. Reed, L. A. Curtiss, and F. Weinhold, *Chem. Rev.*, 1988, **88**, 899–926.
81. E. R. Johnson, S. Keinan, P. Mori-Sánchez, J. Contreras-García, A. J. Cohen, and W. Yang, *J. Am. Chem. Soc.*, 2010, **132**, 6498–6506.
82. U. Koch and P. L. A. Popelier, *J. Chem. Phys.*, 1995, **99**, 9747–9754.
83. S. J. Grabowski, *Chem. Rev.*, 2011, **111**, 2597–2625.
84. C. Garau, A. Frontera, D. Quiñero, P. Ballester, A. Costa, and P. M. Deyà, *J. Phys. Chem. A*, 2004, **108**, 9423–9427.
85. A. Hassan, T. C. Dinadayalane, S. J. Grabowski, and J. Leszczynski, *Phys. Chem. Chem. Phys.*, 2013, **15**, 20839–20856.
86. C. Garau, A. Frontera, D. Quiñero, P. Ballester, A. Costa, and P. M. Deyà, *ChemPhysChem*, 2003, **4**, 1344–1348.
87. A. Ebrahimi, M. Habibi-Khorassani, A. R. Gholipour, and H. R. Masoodi, *Theor Chem Account*, 2009, **124**, 115–122.
88. L. R. Rutledge, C. D. M. Churchill, and S. D. Wetmore, *J Phys Chem B*, 2010, **114**, 3355–3367.
89. A. Mohajeri and E. Karimi, *Journal of Molecular Structure: THEOCHEM*, 2006, **774**, 71–76.
90. F. Blanco, B. Kelly, I. Alkorta, I. Rozas, and J. Elguero, *Chem. Phys. Lett.*, 2011, **511**, 129–134.
91. P. B. Lutz and C. A. Bayse, *Phys. Chem. Chem. Phys.*, 2013, **15**, 9397–9406.
92. Y. Wang, H. Li, and S. Han, *J. Chem. Phys.*, 2006, **124**, 044504.
93. L. del Olmo, C. Morera-Boado, R. López, and J. M. García de la Vega, *J Mol Model*, 2014, **20**, 2175.
94. Y. Gao, L. Zhang, Y. Wang, and H. Li, *J Phys Chem B*, 2010, **114**, 2828–2833.
95. W. Wu, Y. Lu, Y. Liu, H. Li, C. Peng, H. Liu, and W. Zhu, *J. Phys. Chem. A*, 2014, **118**, 2508–2518.
96. J. N. Canongia Lopes, J. Deschamps, and A. A. H. Pádua, *J Phys Chem B*, 2004, **108**, 2038–2047.
97. E. J. Maginn, *Acc. Chem. Res.*, 2007, **40**, 1200–1207.
98. E. J. Maginn, *J Phys Condens Matter*, 2009, **21**, 373101.
99. T. I. Morrow and E. J. Maginn, *J Phys Chem B*, 2002, **106**, 12807–12813.
100. B. L. Bhargava and S. Balasubramanian, *J. Chem. Phys.*, 2007, **127**, 114510.
101. V. Chaban, *Phys. Chem. Chem. Phys.*, 2011, **13**, 16055–16062.
102. T. Yan, C. J. Burnham, M. G. Del Pópolo, and G. A. Voth, *J Phys Chem B*, 2004, **108**, 11877–11881.
103. K. Wendler, F. Dommert, Y. Y. Zhao, R. Berger, C. Holm, and L. Delle Site, *Faraday Discuss.*, 2012, **154**, 111–32– discussion 189–220–

- 465–71.
104. C. J. Cramer, *Essentials of Computational Chemistry*, John Wiley & Sons, 2013.
105. F. Martin and H. Zipse, *J. Comput. Chem.*, 2005, **26**, 97–105.
106. A. Stone, *The Theory of Intermolecular Forces*, Oxford University Press, 2013.
107. E. Sigfridsson and U. Ryde, *J. Comput. Chem.*, 1998, **19**, 377–395.
108. M. Mantina, A. C. Chamberlin, R. Valero, C. J. Cramer, and D. G. Truhlar, *J. Phys. Chem. A*, 2009, **113**, 5806–5812.
109. R. F. W. Bader and C. F. Matta, *J. Phys. Chem. A*, 2004, **108**, 8385–8394.
110. M. J. Frisch, G. W. Trucks, H. B. Schlegel, G. E. Scuseria, M. A. Robb, J. R. Cheeseman, G. Scalmani, V. Barone, B. Mennucci, G. A. Petersson, H. Nakatsuji, M. Caricato, X. Li, H. P. Hratchian, A. F. Izmaylov, J. Bloino, G. Zheng, J. L. Sonnenberg, M. Hada, M. Ehara, K. Toyota, R. Fukuda, J. Hasegawa, M. Ishida, T. Nakajima, Y. Honda, O. Kitao, H. Nakai, T. Vreven, J. A. Montgomery Jr, J. E. Peralta, F. Ogliaro, M. Bearpark, J. J. Heyd, E. Brothers, K. N. Kudin, V. N. Staroverov, R. Kobayashi, J. Normand, K. Raghavachari, A. Rendell, J. C. Burant, S. S. Iyengar, J. Tomasi, M. Cossi, N. Rega, J. M. Millam, M. Klene, J. E. Knox, J. B. Cross, V. Bakken, C. Adamo, J. Jaramillo, R. Gomperts, R. E. Stratmann, O. Yazyev, A. J. Austin, R. Cammi, C. Pomelli, J. W. Ochterski, R. L. Martin, K. Morokuma, V. G. Zakrzewski, G. A. Voth, P. Salvador, J. J. Dannenberg, S. Dapprich, A. D. Daniels, Ö. Farkas, J. B. Foresman, J. V. Ortiz, J. Cioslowski, and D. J. Fox, *Gaussian*, 2009.
111. S. Grimme, W. Hujo, and B. Kirchner, *Phys. Chem. Chem. Phys.*, 2012, **14**, 4875–4883.
112. S. Zahn and B. Kirchner, *J. Phys. Chem. A*, 2008, **112**, 8430–8435.
113. S. Zahn, D. R. MacFarlane, and E. I. Izgorodina, *Phys. Chem. Chem. Phys.*, 2013, **15**, 13664–13675.
114. R. Dennington, T. Keith, and J. Millam, *Semichem Inc: Shawnee Mission*, 2009.
115. E. D. Glendening, J. K. Badenhoop, A. E. Reed, J. E. Carpenter, J. A. Bohmann, C. M. Morales, and F. Weinhold, *Theoretical Chemistry Institute, University of Wisconsin, Madison (2001)*, 2001.
116. T. A. Keith, *Version 131104, TK Gristmill Software, Overland Park KS, USA*, 2013.
117. J. Contreras-García, E. R. Johnson, S. Keinan, R. Chaudret, J.-P. Piquemal, D. N. Beratan, and W. Yang, *J. Chem. Theory Comput.*, 2011, **7**, 625–632.
118. W. Humphrey, A. Dalke, and K. Schulten, *Journal of Molecular Graphics*, 1996, **14**, 33–38.
119. F. Weinhold and C. R. Landis, *Valency and Bonding*, Cambridge University Press, 2005.
120. E. I. Izgorodina, U. L. Bernard, and D. R. MacFarlane, *J. Phys. Chem. A*, 2009, **113**, 7064–7072.
121. E. A. Turner, C. C. Pye, and R. D. Singer, *J. Phys. Chem. A*, 2003, **107**, 2277–2288.
122. S. Tsuzuki, A. A. Arai, and K. Nishikawa, *J Phys Chem B*, 2008, **112**, 7739–7747.
123. C. J. Dymek Jr., D. A. Grossie, A. V. Fratini, and W. Wade Adams, *J. Mol. Struct.*, 1989, **213**, 25–34.
124. V. Kemper and B. Kirchner, *J. Mol. Struct.*, 2010, **972**, 22–34.
125. A. Khrizman, H. Y. Cheng, G. Bottini, and G. Moyna, *Chem. Comm.*, 2015, **51**, 3193–3195.
126. M. O. Sinnokrot and C. D. Sherrill, *J. Phys. Chem. A*, 2006, **110**, 10656–10668.
127. D. CREMER and E. KRAKA, *Croatica Chemica Acta*, 1984, **57**, 1259–1281.
128. L. Sobczyk, S. J. Grabowski, and T. M. Krygowski, *Chem. Rev.*, 2005, **105**, 3513–3560.
129. S. Jenkins and I. Morrison, *Chem. Phys. Lett.*, 2000, **317**, 97–102.
130. R. M. Lynden-Bell, *Phys. Chem. Chem. Phys.*, 2010, **12**, 1733–1740.
131. J. Gao, D. G. Truhlar, Y. Wang, M. J. M. Mazack, P. Löffler, M. R. Provorso, and P. Rehak, *Acc. Chem. Res.*, 2014, **47**, 2837–2845.
132. N. R. Dhumal, H. J. Kim, and J. Kiefer, *J. Phys. Chem. A*, 2009, **113**, 10397–10404.
133. N. R. Dhumal, K. Noack, J. Kiefer, and H. J. Kim, *J. Phys. Chem. A*, 2014, **118**, 2547–2557.